Shape functions for velocity interpolation in general hexahedral cells

R.L. Naff (rlnaff@usgs.gov)
U.S. Geological Survey, Denver, CO USA

T.F. Russell (trussell@carbon.cudenver.edu) *
University of Colorado at Denver, Denver, CO USA

J.D. Wilson (johndw@usgs.gov)†
University of Colorado at Denver, Denver, CO USA

Abstract. Numerical methods for grids with irregular cells require discrete shape functions to approximate the distribution of quantities across cells. For control-volume mixed finite-element (CVMFE) methods, vector shape functions approximate velocities and vector test functions enforce a discrete form of Darcy's law. In this paper, a new vector shape function is developed for use with irregular, hexahedral cells (trilinear images of cubes). It interpolates velocities and fluxes quadratically, because as shown here, the usual Piola-transformed shape functions, which interpolate linearly, cannot match uniform flow on general hexahedral cells. Truncation-error estimates for the shape function are demonstrated. CVMFE simulations of uniform and non-uniform flow with irregular meshes show first- and second-order convergence of fluxes in the L^2 norm in the presence and absence of singularities, respectively.

1. INTRODUCTION

For simulation of two-dimensional (2-D) flow in heterogeneous porous media, it has been shown that mixed methods, and in particular the control-volume mixed finite-element (CVMFE) method [1], can be efficient, accurate schemes to obtain the velocity field [1–3]. As part of an extension of CVMFE to 3-D, here we develop and test a 3-D CVMFE velocity shape function for irregular hexahedral cells, based on covariant vectors for a mapping to a unit cube. Its performance is evaluated with the L^2 norm of the flux error in a number of test cases.

In 3-D CVMFE, the domain is discretized into potentially irregular hexahedral cells, allowing for the modeling of complex hydrogeological systems. Vector shape functions, described subsequently, interpolate the velocity over the interiors of cells, and vector test functions are weighting factors in integrating the Darcy relation over control volumes associated with cell faces; this can be viewed as an error minimization in the control-volume technique [4]. The shape and test functions result in discrete equations that can be solved for fluxes at cell faces and pressures at cell centers. Shape functions interpolate cell-surface fluxes, approximating the velocity in the cell interior; a poor approximation degrades the solution. We propose a new velocity shape function for 3-D logically rectangular meshes which, in most cases, should provide a reasonable cell-velocity estimate. This function is based on a second-order approximation of flux conservation across the cell, which can be a non-linear interpolation of the flux and the velocity. For 3-D flow on irregular meshes, we believe that this function will offer advantages over 3-D versions of the 2-D linear shape function in [1].

Sections 2–5 provide background on the problem and the solution technique. In particular, section 3 describes the roles of the shape functions and test functions in CVMFE. Section 4 shows that the flux of a uniform flow field across an arbitrary cell is not necessarily linear; this affects the construction of the shape functions. Section 5 discusses the Piola transformation, which determines standard shape functions with linear flux for irregular cells. Velocity interpolation functions, a precursor of the shape functions, are presented in section 6, followed by the shape functions themselves in section 7. Sections 8 and 9 present results of the velocity shape function for uniform and non-uniform flow, respectively. A brief discussion of the results concludes the paper.

* Supported in part by NSF Grants DMS-9706866 and DMS-0084438 and ARO Grant 37119-GS-AAS.
† Presently at: U.S. Geological Survey, Denver, CO USA

Report Documentation Page

Form Approved
OMB No. 0704-0188

1. REPORT DATE	2. REPORT TYPE	3. DATES COVERED
2001		**00-00-2001 to 00-00-2001**

4. TITLE AND SUBTITLE	5a. CONTRACT NUMBER
Shape Functions for Velocit Interpolation in General Hexahedral Cells	5b. GRANT NUMBER
	5c. PROGRAM ELEMENT NUMBER
6. AUTHOR(S)	5d. PROJECT NUMBER
	5e. TASK NUMBER
	5f. WORK UNIT NUMBER
7. PERFORMING ORGANIZATION NAME(S) AND ADDRESS(ES) **University of Colorado at Denver,Center for Computational Mathematics,PO Box 173364,Denver,CO,80217-3364**	8. PERFORMING ORGANIZATION REPORT NUMBER
9. SPONSORING/MONITORING AGENCY NAME(S) AND ADDRESS(ES)	10. SPONSOR/MONITOR'S ACRONYM(S)
	11. SPONSOR/MONITOR'S REPORT NUMBER(S)

12. DISTRIBUTION/AVAILABILITY STATEMENT
Approved for public release; distribution unlimited

13. SUPPLEMENTARY NOTES

14. ABSTRACT
see report

15. SUBJECT TERMS

16. SECURITY CLASSIFICATION OF:			17. LIMITATION OF ABSTRACT	18. NUMBER OF PAGES	19a. NAME OF RESPONSIBLE PERSON
a. REPORT **unclassified**	b. ABSTRACT **unclassified**	c. THIS PAGE **unclassified**		**22**	

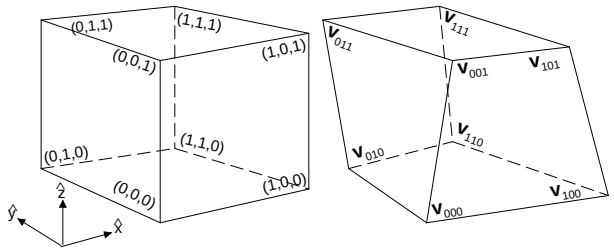

Figure 1. Left: reference cube $\hat{Q}$ with edges of unit length. Right: arbitrary cell Q from discretization with vertex locations $\mathbf{v}_{000}$, $\mathbf{v}_{100}$, $\mathbf{v}_{010}$, $\mathbf{v}_{001}$, $\mathbf{v}_{110}$, $\mathbf{v}_{101}$, $\mathbf{v}_{011}$ and $\mathbf{v}_{111}$ indicated.

2. BASIC EQUATIONS

This paper applies CVMFE to a steady flow equation in a 3-D domain Ω:

$$\nabla \cdot \mathbf{q} \;=\; W(x,y,z), \qquad (x,y,z) \in \Omega. \tag{1}$$

Here $\mathbf{q}$ is the specific discharge vector and W is a source term. Boundary conditions on the surface $\partial\Omega$ are fluxes over $\partial\Omega_f$ and/or specified pressures over $\partial\Omega_p$. We assume the Darcy relation:

$$\mathbf{q} \;=\; -\mathbf{K}\nabla p \,/\, \mu, \tag{2}$$

where p is the pressure, $\mathbf{K}(x,y,z)$ is the hydraulic conductivity tensor and μ is the viscosity (the gravitational potential is neglected from (2) for notational convenience). Like most mixed methods, CVMFE inverts the hydraulic conductivity tensor in (2), so that

$$\nabla p \;=\; -\mu\mathbf{K}^{-1}\mathbf{q}. \tag{3}$$

The mixed-method development herein uses (1) and (3) as a basis of the numerical approximation.

We discretize Ω with a logically rectangular mesh of hexahedral cells. Each cell Q is the image under a trilinear mapping of a regular reference hexahedron (unit cube), $\hat{Q}$; Q is determined by its vertices at $\mathbf{v}_{000}$, $\mathbf{v}_{100}$, $\mathbf{v}_{010}$, $\mathbf{v}_{001}$, $\mathbf{v}_{110}$, $\mathbf{v}_{101}$, $\mathbf{v}_{011}$ and $\mathbf{v}_{111}$, where $\mathbf{v}_{\alpha\beta\gamma} = (x_{\alpha\beta\gamma}, y_{\alpha\beta\gamma}, z_{\alpha\beta\gamma})$ (Figure 1). Note that the faces of Q may be non-planar. The mapping associates with any reference location $\hat{\mathbf{r}} = (\hat{x},\hat{y},\hat{z})$ in $\hat{Q}$, the point $\mathbf{r} = (x,y,z)$ in Q:

$$\mathbf{r} \;=\; \mathbf{v}_o + \mathbf{v}_a\hat{x} + \mathbf{v}_b\hat{y} + \mathbf{v}_c\hat{z} + \mathbf{v}_d\hat{x}\hat{y} + \mathbf{v}_e\hat{x}\hat{z} + \mathbf{v}_f\hat{y}\hat{z} + \mathbf{v}_g\hat{x}\hat{y}\hat{z}, \tag{4}$$

where $\mathbf{v}_o = \mathbf{v}_{000}$, $\mathbf{v}_a = \mathbf{v}_{100} - \mathbf{v}_o$, $\mathbf{v}_b = \mathbf{v}_{010} - \mathbf{v}_o$, $\mathbf{v}_c = \mathbf{v}_{001} - \mathbf{v}_o$, $\mathbf{v}_d = \mathbf{v}_{110} - \mathbf{v}_o - \mathbf{v}_a - \mathbf{v}_b$, $\mathbf{v}_e = \mathbf{v}_{101} - \mathbf{v}_o - \mathbf{v}_a - \mathbf{v}_c$, $\mathbf{v}_f = \mathbf{v}_{011} - \mathbf{v}_o - \mathbf{v}_b - \mathbf{v}_c$, $\mathbf{v}_g = \mathbf{v}_{111} - \mathbf{v}_o - \mathbf{v}_a - \mathbf{v}_b - \mathbf{v}_c - \mathbf{v}_d - \mathbf{v}_e - \mathbf{v}_f$. This mapping extends the conventional bilinear mapping for a logically rectangular grid [1, 5]. Note that a fixed $\hat{x}$ in $\hat{Q}$ determines a face normal to the $\hat{x}$ direction, which (4) maps into a corresponding face within Q. Covariant vectors, defined as $\mathbf{X}(\hat{y},\hat{z}) \equiv \partial\mathbf{r}/\partial\hat{x}$, $\mathbf{Y}(\hat{x},\hat{z}) \equiv \partial\mathbf{r}/\partial\hat{y}$ and $\mathbf{Z}(\hat{x},\hat{y}) \equiv \partial\mathbf{r}/\partial\hat{z}$, describe the geometry of Q. The volumetric Jacobian J for passing from Q to $\hat{Q}$ is simply [6]

$$J(\hat{x},\hat{y},\hat{z}) \;=\; \mathbf{X}(\hat{y},\hat{z}) \cdot (\mathbf{Y}(\hat{x},\hat{z}) \times \mathbf{Z}(\hat{x},\hat{y})), \tag{5}$$

while, for a face in the logical x direction, the surface Jacobian Γ_x becomes [6]

$$\Gamma_x(\hat{x},\hat{y},\hat{z}) \;=\; |\mathbf{Y}(\hat{x},\hat{z}) \times \mathbf{Z}(\hat{x},\hat{y})|, \tag{6}$$

and the unit normal to this surface is

$$\mathbf{n}_{\hat{x}} = (\mathbf{Y} \times \mathbf{Z}) \,/\, |\mathbf{Y} \times \mathbf{Z}|. \tag{7}$$

Surface Jacobians and unit normals are similarly defined for faces in the logical y and z directions. These relations allow us to define the necessary quantities used within the CVMFE method.

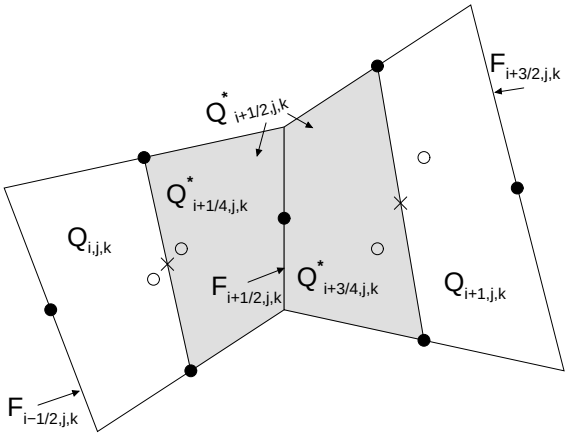

Figure 2. Midsection through two adjoining cells in the logical x direction. Filled and open circles represent locations on faces where fluxes are estimated; open circles represent flux locations on faces in the logical y direction projected onto midsection. The $\times$ symbol is used to denote pressure locations at logical cell centers.

3. CVMFE METHOD

The CVMFE method uses velocity basis vectors $\mathbf{v}_{i,j,k;m,n,p}(\mathbf{r})$ to approximate the Darcy velocity $\mathbf{q}$ in a cell $Q_{i,j,k}$ from the bulk cell-face fluxes. Here, i, j, k index the cell's position in the mesh, while m, n, p determine a face $F_{i+m,j+n,k+p}$ of $Q_{i,j,k}$. Then the approximation of $\mathbf{q}$ in $Q_{i,j,k}$ can be written

$$\begin{aligned}\mathbf{q} \;\approx\;& f_{i+1/2,j,k}\,\mathbf{v}_{i,j,k;1/2,0,0} + f_{i-1/2,j,k}\,\mathbf{v}_{i,j,k;-1/2,0,0} + f_{i,j+1/2,k}\,\mathbf{v}_{i,j,k;0,1/2,0} \\ &+\; f_{i,j-1/2,k}\,\mathbf{v}_{i,j,k;0,-1/2,0} + f_{i,j,k+1/2}\,\mathbf{v}_{i,j,k;0,0,1/2} + f_{i,j,k-1/2}\,\mathbf{v}_{i,j,k;0,0,-1/2},\end{aligned} \tag{8}$$

where, for example, $f_{i+1/2,j,k}$ is the bulk flux through face $F_{i+1/2,j,k}$. Here, note that "flux" is defined to be the total volumetric discharge through a cell face, as opposed to the volumetric discharge per unit area, which is typical in the fluid mechanics literature. Substitute (8) into (1) and integrate both sides over $Q_{i,j,k}$; the desired result is

$$f_{i+1/2,j,k} - f_{i-1/2,j,k} + f_{i,j+1/2,k} - f_{i,j-1/2,k} + f_{i,j,k+1/2} - f_{i,j,k-1/2} \;=\; \int_{Q_{i,j,k}} W(x,y,z)\,dxdydz. \tag{9}$$

To obtain (9), by the Gauss divergence theorem the shape functions must satisfy

$$\int_{Q_{i,j,k}} \nabla\cdot\mathbf{v}_{i,j,k;m,n,p}\,dxdydz \;=\; \pm 1. \tag{10}$$

Thus, the shape functions should yield a discrete form (9) of the continuity equation (1) in Ω.

To develop a discrete form for the Darcy relation (3), a control volume which straddles a cell face $F_{i+m,j+n,k+p}$ is used; control volume $Q^*_{i+1/2,j,k}$ for face $F_{i+1/2,j,k}$ is depicted in Figure 2. Weighted with a test function $\mathbf{w}_{i+1/2,j,k}$, and with $\mathbf{q}$ approximated by (8), (3) is integrated over $Q^*_{i+1/2,j,k}$. The choice of the test function is motivated by the efficiency and convenience of eliminating face pressures adjoining two cells; see [4]. Here, we use the form proposed by Garanzha and Konshin [5] for the test function, a modification of that originally described in [1], as we have found that it performs well in most cases [4]. Referring to face $F_{i+1/2,j,k}$ of Figure 2, this test function is

$$\mathbf{w}_{i+1/2,j,k} \;=\; \begin{cases} \mathbf{X}_{i,j,k}(\hat{y},\hat{z})/J_{i,j,k}(\hat{x},\hat{y},\hat{z}), & \text{on } Q^*_{i+1/4,j,k}, \\ \mathbf{X}_{i+1,j,k}/J_{i+1,j,k}, & \text{on } Q^*_{i+3/4,j,k}, \\ 0, & \text{otherwise,} \end{cases} \tag{11}$$

where $\mathbf{X}_{i,j,k}$ is the covariant vector for $\partial\mathbf{r}/\partial\hat{x}$. Similar forms exist for the logical y and z directions.

Over the straddling control volume $Q^*_{i+1/2,j,k}$ the specific discharge approximation analogous to (8) involves the two adjoining cells; allowing $\mathbf{V}_{i+1/2,j,k}$ to be this approximator, then

$$\begin{aligned}\mathbf{V}_{i+1/2,j,k} &= f_{i+1/2,j,k}\left(\boldsymbol{\nu}_{i,j,k;1/2,0,0}+\boldsymbol{\nu}_{i+1,j,k;-1/2,0,0}\right)+f_{i-1/2,j,k}\boldsymbol{\nu}_{i,j,k;-1/2,0,0}\\ &+ f_{i+3/2,j,k}\boldsymbol{\nu}_{i+1,j,k;1/2,0,0}+f_{i,j+1/2,k}\boldsymbol{\nu}_{i,j,k;0,1/2,0}+f_{i,j-1/2,k}\boldsymbol{\nu}_{i,j,k;0,-1/2,0}\\ &+ f_{i,j,k+1/2}\boldsymbol{\nu}_{i,j,k;0,0,1/2}+f_{i,j,k-1/2}\boldsymbol{\nu}_{i,j,k;0,0,-1/2}+f_{i+1,j+1/2,k}\boldsymbol{\nu}_{i+1,j,k;0,1/2,0}\\ &+ f_{i+1,j-1/2,k}\boldsymbol{\nu}_{i+1,j,k;0,-1/2,0}+f_{i+1,j,k+1/2}\boldsymbol{\nu}_{i+1,j,k;0,0,1/2}+f_{i+1,j,k-1/2}\boldsymbol{\nu}_{i+1,j,k;0,0,-1/2}. \quad (12)\end{aligned}$$

The discrete Darcy relation is obtained from (3) by integrating (12) against (11) over $Q^*_{i+1/2,j,k}$:

$$p_{i+1,j,k}-p_{i,j,k} = -\mu\int_{Q^*_{i+1/2,j,k}}\left(\mathbf{K}^{-1}\mathbf{V}_{i+1/2,j,k}\right)\cdot\mathbf{w}_{i+1/2,j,k}\,dxdydz. \quad (13)$$

The integrations in (13) result in a set of coefficients relating the bulk fluxes on the faces of $Q_{i,j,k}$ and $Q_{i+1,j,k}$ to the difference in pressures at the cell centers (at $\hat{x}=\hat{y}=\hat{z}=1/2$ in each cell). This method is applied to all interior faces of the domain, forming a discrete Darcy relation (13) for each face. The discrete continuity and Darcy equations, (9) and (13), applied to every cell within the domain, form the discretizations for the CVMFE method. With irregular grids, this system of equations can be non-symmetric, though with certain numerical integration rules symmetry can be assured [5]; otherwise, it is similar in structure to equations that result from other mixed-method techniques.

On a uniform grid with a scalar conductivity $\mathbf{K}$, with the shape functions of the usual mixed method and with control-volume test functions as in (11), the integrations in (13) lead to a tridiagonal mass matrix with coefficients in the proportion of 1/8, 6/8, 1/8. For the usual mixed method, in which the test functions are the same as the shape functions, the analogous proportions are 1/6, 4/6, 1/6, and for the usual finite-volume or finite-difference methods, they are 0, 1, 0 (diagonal or lumped mass matrix). As pointed out in [5], based on one-sided compact difference schemes, the off-diagonal coefficient 1/8 of CVMFE can be expected to preserve second-order accuracy on non-uniform grids, in which there is no particular relation between the grids on the two sides of an interface. This may be the reason why CVMFE has calculated second-order-accurate fluxes on non-smooth quadrilateral grids in 2-D, without any need for Lagrange multipliers (corresponding to face pressures) as in the usual mixed methods (e.g., [7]).

4. FLUX INTERPOLATION

This section discusses interpolation of cell-face fluxes over cell interiors, a prelude to developing cell-velocity interpolation functions. Consider the flux $f_x(\hat{x})$ across an interior cell surface defined by a fixed value of $\hat{x}$ within $\hat{Q}$; if f_x is the result of a velocity field $\mathbf{q}(\mathbf{r})$, then this flux is:

$$f_x(\hat{x}) = \int_{\hat{x}}\mathbf{q}(\mathbf{r})\cdot\mathbf{n}_{\hat{x}}\,dS = \int_0^1\int_0^1\mathbf{q}(\hat{\mathbf{r}})\cdot\mathbf{n}_{\hat{x}}|\mathbf{Y}\times\mathbf{Z}|\,d\hat{y}d\hat{z} = \int_0^1\int_0^1\mathbf{q}(\hat{x},\hat{y},\hat{z})\cdot(\mathbf{Y}\times\mathbf{Z})(\hat{x},\hat{y},\hat{z})\,d\hat{y}d\hat{z}, \quad (14)$$

where $\mathbf{n}_{\hat{x}}$ is the unit normal to this surface (7). The cross product $\mathbf{Y}\times\mathbf{Z}$ is a function of $\hat{\mathbf{r}}=(\hat{x},\hat{y},\hat{z})$ and represents a pole normal to the surface at $\hat{x}$. Its dependency on $\hat{x}$ can be made explicit (see Appendix A):

$$\mathbf{Y}\times\mathbf{Z} = (1-\hat{x})(\mathbf{Y}_{0x}\times\mathbf{Z}_{0x})+\hat{x}(\mathbf{Y}_{1x}\times\mathbf{Z}_{1x})-\hat{x}(1-\hat{x})(\mathbf{Y}_{2x}\times\mathbf{Z}_{2x}), \quad (15)$$

where $\mathbf{Y}_{0x}(\hat{z})=\mathbf{Y}|_{\hat{x}=0}$, $\mathbf{Z}_{0x}(\hat{y})=\mathbf{Z}|_{\hat{x}=0}$, $\mathbf{Y}_{1x}(\hat{z})=\mathbf{Y}|_{\hat{x}=1}$, $\mathbf{Z}_{1x}(\hat{y})=\mathbf{Z}|_{\hat{x}=1}$, $\mathbf{Y}_{2x}=\mathbf{Y}_{1x}-\mathbf{Y}_{0x}$, and $\mathbf{Z}_{2x}=\mathbf{Z}_{1x}-\mathbf{Z}_{0x}$. Substituting (14) into (15), the bulk flux across the surface at $\hat{x}$ is

$$f_x(\hat{x}) = (1-\hat{x})\,f_{0x}(\hat{x})+\hat{x}\,f_{1x}(\hat{x})-\hat{x}(1-\hat{x})\,f_{2x}(\hat{x}), \quad (16)$$

where

$$f_{0x}(\hat{x}) = \int_0^1 \int_0^1 \mathbf{q}(\hat{x},\hat{y},\hat{z}) \cdot (\mathbf{Y}_{0x} \times \mathbf{Z}_{0x})\, d\hat{y} d\hat{z}, \tag{17a}$$

$$f_{1x}(\hat{x}) = \int_0^1 \int_0^1 \mathbf{q}(\hat{x},\hat{y},\hat{z}) \cdot (\mathbf{Y}_{1x} \times \mathbf{Z}_{1x})\, d\hat{y} d\hat{z}, \tag{17b}$$

$$f_{2x}(\hat{x}) = \int_0^1 \int_0^1 \mathbf{q}(\hat{x},\hat{y},\hat{z}) \cdot (\mathbf{Y}_{2x} \times \mathbf{Z}_{2x})\, d\hat{y} d\hat{z}. \tag{17c}$$

For a uniform flow field $\mathbf{q}(\hat{\mathbf{r}}) \equiv \mathbf{q}$, $(17a)$–$(17c)$ are independent of $\hat{x}$. Since f_{0x} and f_{1x} involve both $\mathbf{Y}$ and $\mathbf{Z}$ at $\hat{x} = 0$ and $\hat{x} = 1$, respectively, and f_{2x} is balanced between $\hat{x} = 0$ and $\hat{x} = 1$, it is natural to consider the quadratic approximation

$$Q f_x(\hat{x}) = (1-\hat{x}) f_{0x}(0) + \hat{x} f_{1x}(1) - \hat{x}(1-\hat{x}) f_{2x}(1/2), \tag{18}$$

which is exact for uniform $\mathbf{q}$. We will also make use of the linear approximation

$$L f_x(\hat{x}) = (1-\hat{x}) f_{0x}(0) + \hat{x} f_{1x}(1). \tag{19}$$

The errors of these approximations are derived in Appendix B, which we summarize here. To see the dependence on grid size, scale the x-dimension to Δx, keeping $\hat{y}$ and $\hat{z}$ on the unit interval. (We want to see how the flux error across a fixed x-face varies with Δx; refining it in y and z would have no effect, as we would integrate in y and z over each subface and would sum over them.) For fixed x, $0 \le x \le \Delta x$, the Green's function of the operator d^2/dx^2 with homogeneous Dirichlet boundary conditions is

$$G(x,\xi) = \begin{cases} \xi\left(\frac{x}{\Delta x} - 1\right), & 0 \le \xi \le x, \\ x\left(\frac{\xi}{\Delta x} - 1\right), & x \le \xi \le \Delta x. \end{cases} \tag{20}$$

Now $f_x - L f_x$ satisfies these boundary conditions and $(L f_x)'' \equiv 0$, so that

$$f_x(x) - L f_x(x) = \int_0^{\Delta x} G(x,\xi) \left(\frac{d^2}{dx^2}(f_x - L f_x) \right)(\xi)\, d\xi = \int_0^{\Delta x} G(x,\xi)\, f_x''(\xi)\, d\xi. \tag{21}$$

In Appendix B, it is shown that (21) leads to

$$\begin{aligned}
&(f_x - Q f_x)(x) \\
&= \int_0^{\Delta x} G(x,\xi) \int_0^1 \int_0^1 \left\{ \frac{2}{\Delta x} \frac{\partial \mathbf{q}}{\partial x}(\xi,\hat{y},\hat{z}) \cdot (\mathbf{Y}_{1x} \times \mathbf{Z}_{1x} - \mathbf{Y}_{0x} \times \mathbf{Z}_{0x}) \right. \\
&\quad + \left(1 - \frac{\xi}{\Delta x}\right) \frac{\partial^2 \mathbf{q}}{\partial x^2}(\xi,\hat{y},\hat{z}) \cdot (\mathbf{Y}_{0x}(\hat{z}) \times \mathbf{Z}_{0x}(\hat{y})) + \frac{\xi}{\Delta x} \frac{\partial^2 \mathbf{q}}{\partial x^2}(\xi,\hat{y},\hat{z}) \cdot (\mathbf{Y}_{1x}(\hat{z}) \times \mathbf{Z}_{1x}(\hat{y})) \\
&\quad + \left[\frac{2}{\Delta x^2} \left(\mathbf{q}(\xi,\hat{y},\hat{z}) - \mathbf{q}\left(\frac{\Delta x}{2},\hat{y},\hat{z}\right) \right) + \frac{4}{\Delta x} \left(\frac{\xi}{\Delta x} - \frac{1}{2} \right) \frac{\partial \mathbf{q}}{\partial x}(\xi,\hat{y},\hat{z}) - \frac{\xi}{\Delta x} \left(1 - \frac{\xi}{\Delta x}\right) \frac{\partial^2 \mathbf{q}}{\partial x^2}(\xi,\hat{y},\hat{z}) \right] \cdot \\
&\quad \left. \cdot (\mathbf{Y}_{2x}(\hat{z}) \times (\mathbf{Z}_{2x}(\hat{y})) \right\} d\hat{y} d\hat{z} d\xi
\end{aligned} \tag{22}$$

and

$$\begin{aligned}
(f_x - L f_x)(x) = (f_x - Q f_x)(x) + \int_0^{\Delta x} G(x,\xi) \int_0^1 \int_0^1 \frac{2}{\Delta x^2} \mathbf{q}\left(\frac{\Delta x}{2},\hat{y},\hat{z}\right) \cdot \\
\cdot (\mathbf{Y}_{2x}(\hat{z}) \times \mathbf{Z}_{2x}(\hat{y}))\, d\hat{y} d\hat{z} d\xi.
\end{aligned} \tag{23}$$

Assuming smooth variation of $\mathbf{q}$, $\mathbf{Y}$, and $\mathbf{Z}$ with x, the errors in (22) and (23) are both $O(\Delta x^2)$, with the two powers of Δx coming from the $d\xi$ integral and the Green's function. The $\partial\mathbf{q}/\partial x$ and $\mathbf{q}$ terms have coefficients that are $O(\Delta x^{-1})$ and $O(\Delta x^{-2})$, respectively, but in each case they are multiplied by a difference or product of differences that restores the power(s) of Δx.

Note that $\mathbf{q}$ appears in $f_x - Lf_x$, while $f_x - Qf_x$ has only derivatives and differences of $\mathbf{q}$. Thus, Qf_x yields exact fluxes for uniform $\mathbf{q}$, while Lf_x does not, though both are second-order. The second-order terms in $f_x - Qf_x$ are the first two $\partial^2\mathbf{q}/\partial x^2$ terms, present even on a uniform cartesian grid (i.e., unavoidable unless $\mathbf{q}$ is linear), and the first $\partial\mathbf{q}/\partial x$ term, due only to grid distortion and vanishing if x-faces were uniform. In $f_x - Lf_x$ there is also the second-order term in (23).

The above analysis tacitly assumes that the coarse-cell refinement is smooth, e.g., along the trilinear coordinates set up by the reference mapping (the coarse grid may be rough; only the asymptotic refinement of each cell need be smooth). If so, then $\mathbf{Y}_2$, $\mathbf{Z}_2$, and the difference of $\mathbf{Y}\times\mathbf{Z}$ in (22) are all $O(\Delta x)$. Equivalently, in a refined coarse cell, the angular deviation from a parallelepiped is assumed to decrease as $O(\Delta x)$ (so that the deviation of the vertices decreases as $O(\Delta x^2)$). If not, i.e., if angular deviations do not decrease ("random" refinement), then $\mathbf{Y}_2$, $\mathbf{Z}_2$, and the difference of $\mathbf{Y}\times\mathbf{Z}$ are $O(1)$. In $f_x - Qf_x$, the $\partial\mathbf{q}/\partial x$ and $\mathbf{q}$ (difference) terms become first-order; in $f_x - Lf_x$, the $\mathbf{q}$ term becomes zeroth-order. Thus, along with its exact interpolation of uniform-flow fluxes on distorted grids, the quadratic flux interpolation may be crucial in obtaining convergent flux approximations on randomly refined grids.

The next section shows that the Piola transformation, commonly used to relate vector-valued functions on reference cells to irregular hexahedral cells, leads to the linear flux interpolation Lf_x. The possible shortcomings of Lf_x noted here will motivate consideration of shape functions other than those obtained from the Piola transformation.

In (18), the quadratic flux interpolation requires that $f_{0x}(0)$, $f_{1x}(1)$ and $f_{2x}(1/2)$ be known. Fluxes $f_{0x}(0)$ and $f_{1x}(1)$ are components of the solution vector for a mixed method. If the cross product $\mathbf{Y}_{2x}\times\mathbf{Z}_{2x}$ in f_{2x} is taken to be a pole normal to a surface, then $|\mathbf{Y}_{2x}\times\mathbf{Z}_{2x}|d\hat{y}d\hat{z}$ can be viewed as an elemental area on this surface; we adopt this and define the surface as the *secondary face*, as opposed to the *primary faces* formed by the cell surfaces. An approximation of the *secondary flux* $f_{2x}(1/2)$ in terms of primary fluxes will be presented later; here, it is treated as known. If cells are parallelepipeds, the last term in (18) is null as $\mathbf{Y}_{2x}\times\mathbf{Z}_{2x}=\mathbf{0}$; thus, flux interpolation for regular grids will be linear, as for the Piola transformation.

In (17c), $(\hat{y},\hat{z})$ ranges over the square $(0,1)\times(0,1)$. The secondary surface can be *planar* (vector $\mathbf{Y}_{2x}\times\mathbf{Z}_{2x}$ points in the same direction for all $(\hat{y},\hat{z})$), *non-planar* (the direction varies with $(\hat{y},\hat{z})$), or *twisted planar* (the vector points in opposite directions at $(\hat{y},\hat{z})=(0,0)$ and $(1,1)$). For twisted planar faces, expressions such as $|\mathbf{Y}_{2x}\times\mathbf{Z}_{2x}|\,d\hat{y}d\hat{z}$ become suspect because such a face would be excluded in the 2-D mapping from a distorted but convex quadrilateral to the unit square; such mappings are implicit to this work. This behavior affects the accuracy of the cell-velocity interpolation function, discussed in subsequent sections.

5. PIOLA TRANSFORMATION

The Piola transformation relates vector-valued functions on a hexahedron Q to ones on the reference cube $\hat{Q}$ in a manner that preserves normal fluxes across primary cell faces and parts of faces. For velocity interpolation on hexahedral meshes, we must define such functions on Q, given certain values or functionals (e.g., integrated fluxes) of these functions. Let $\mathbf{r}(\hat{x},\hat{y},\hat{z})=\mathbf{r}(\hat{\mathbf{r}})=(x,y,z)$ be as in (4). The Piola transformation takes a vector-valued function $\hat{\mathbf{v}}$ on $\hat{Q}$ to $\mathbf{v}$ on Q defined by

$$\mathbf{v}(\mathbf{r}(\hat{\mathbf{r}})) = \frac{\mathbf{D}\mathbf{r}(\hat{\mathbf{r}})}{J(\hat{\mathbf{r}})}\hat{\mathbf{v}}(\hat{\mathbf{r}}), \tag{24}$$

where $\mathbf{D}\mathbf{r}$ is the Jacobian matrix of $\mathbf{r}$ and the Jacobian J is its determinant. Then [8, 9]

$$\int_{\partial Q}\mathbf{v}\cdot\mathbf{n}(s)\,z(s)\,ds = \int_{\partial\hat{Q}}\hat{\mathbf{v}}\cdot\hat{\mathbf{n}}(\hat{s})\,z(\mathbf{r}(\hat{s}))\,d\hat{s}, \tag{25}$$

where ∂Q is the boundary of Q, $\mathbf{n}(s)$ is the outward unit normal vector at $s \in \partial Q$, z is a scalar-valued function (not necessarily continuous) on ∂Q, and $\hat{\mathbf{n}}(\hat{s})$ is the outward unit normal vector at $\hat{s} \in \partial\hat{Q}$. It is assumed that $\hat{\mathbf{v}}$ and z are smooth enough so that the integrals in (25) make sense; z can be chosen to be 1 on some parts of ∂Q and 0 elsewhere. Thus, (24) preserves normal fluxes across primary cell faces and parts of faces.

We need to generalize (25) to interior faces, such as those for a fixed $\hat{x}$. The standard basis functions on the reference element $\hat{Q}$, associated with primary face fluxes, are the lowest-order Raviart-Thomas (RT_0) functions [10]. Corresponding to the faces $\hat{x} = 0, 1$, $\hat{y} = 0, 1$, $\hat{z} = 0, 1$, respectively, are the velocity fields $\hat{\mathbf{v}}_{x0} = (1-\hat{x}, 0, 0)$, $\hat{\mathbf{v}}_{x1} = (\hat{x}, 0, 0)$, $\hat{\mathbf{v}}_{y0} = (0, 1-\hat{y}, 0)$, $\hat{\mathbf{v}}_{y1} = (0, \hat{y}, 0)$, $\hat{\mathbf{v}}_{z0} = (0, 0, 1-\hat{z})$, $\hat{\mathbf{v}}_{z1} = (0, 0, \hat{z})$. Thus, $\hat{\mathbf{v}}_{x1}$ has flux 1 across the face $\hat{F}_{x1}$ at $\hat{x} = 1$, flux 0 across the other five primary faces, and flux c across interior face $\hat{F}_{xc}$ at $\hat{x} = c$. The normal velocity component is constant on such faces.

Let $\hat{\mathbf{v}} = \hat{\mathbf{v}}_{x1}$, and define $\mathbf{v}$ by (24). Appendix C shows that

$$\int_{F_{xc}} \mathbf{v}\cdot\mathbf{n}\, z\, ds = \int_{\hat{F}_{xc}} c\, z(\mathbf{r}(\hat{s}))\, d\hat{s}, \qquad \int_{F_{yc}} \mathbf{v}\cdot\mathbf{n}\, z\, ds = 0, \tag{26}$$

so that fluxes of $\hat{\mathbf{v}}$ across interior faces and parts of such faces are preserved. By linear combinations, this generalizes at once to any image of an RT_0 function (Piola-transformed velocity) on Q. It follows that the transformed normal component $\mathbf{v}\cdot\mathbf{n}(s)$ on F_{xc} must be $\hat{\mathbf{v}}\cdot\hat{\mathbf{n}}(\hat{s})/\Gamma_{xc}(\hat{s}) = c/\Gamma_{xc}(\hat{s})$, pointwise, where Γ_{xc} denotes the surface Jacobian on F_{xc}, so that $\mathbf{v}\cdot\mathbf{n}$ is proportional to $1/\Gamma_{xc}$. Consider the following two properties of a vector-valued function $\mathbf{q}$ on Q:

(P1) The fluxes $f_x(\hat{x})$, $f_y(\hat{y})$, $f_z(\hat{z})$ vary linearly with $\hat{x}$, $\hat{y}$, $\hat{z}$, respectively.

(P2) The normal components $\mathbf{q}\cdot\mathbf{n}_{\hat{x}}$, $\mathbf{q}\cdot\mathbf{n}_{\hat{y}}$, $\mathbf{q}\cdot\mathbf{n}_{\hat{z}}$ are inversely proportional to the surface Jacobians $|\mathbf{Y}\times\mathbf{Z}|$, $|\mathbf{Z}\times\mathbf{X}|$, $|\mathbf{X}\times\mathbf{Y}|$, respectively.

Then $\mathbf{q}$ *on* Q *is the Piola transform of an* RT_0 *function* $\hat{\mathbf{q}}$ *on* $\hat{Q}$ *if and only if* $\mathbf{q}$ *satisfies (P1) and (P2).*

The "only if" part follows from the linear variation of fluxes of RT_0 functions on $\hat{Q}$ and the flux-preservation properties (26) and generalizations. For the "if" part, let $\mathbf{q}$ satisfy (P1) and (P2). On $\hat{Q}$, there is a unique RT_0 function $\hat{\mathbf{q}}$ with fluxes $f_x(0)$, $f_x(1)$, $f_y(0)$, $f_y(1)$, $f_z(0)$, $f_z(1)$ on the faces $\hat{F}_{x0}$, $\hat{F}_{x1}$, $\hat{F}_{y0}$, $\hat{F}_{y1}$, $\hat{F}_{z0}$, $\hat{F}_{z1}$, respectively. The Piola transform of $\hat{\mathbf{q}}$ satisfies (P1) and (P2), with the same fluxes and normal components as $\mathbf{q}$ everywhere on Q. Since a vector-valued function is uniquely determined by its three normal components at each point, $\mathbf{q}$ must be the Piola transform of $\hat{\mathbf{q}}$. Note that one consequence of this development is that the Piola transformation dictates the linear flux interpolation in (19).

In 2-D, it follows that for any quadrilateral cell Q, a uniform flow $\mathbf{q}$ is the exact Piola transform of an RT_0 function. To see this, let the vertices of Q be $\mathbf{v}_{00}$, $\mathbf{v}_{10}$, $\mathbf{v}_{01}$, $\mathbf{v}_{11}$, with the bilinear mapping

$$\mathbf{r} = (1-\hat{x})(1-\hat{y})\mathbf{v}_{00} + \hat{x}(1-\hat{y})\mathbf{v}_{10} + (1-\hat{x})\hat{y}\mathbf{v}_{01} + \hat{x}\hat{y}\mathbf{v}_{11}. \tag{27}$$

One checks easily that $\mathbf{X} = \mathbf{a} + \hat{y}\mathbf{b}$ and $\mathbf{Y} = \mathbf{c} + \hat{x}\mathbf{d}$, for constant vectors $\mathbf{a}$, $\mathbf{b}$, $\mathbf{c}$, $\mathbf{d}$. The interior edge at fixed $\hat{x}$ is parallel to $\mathbf{Y} = (\partial x/\partial\hat{y}, \partial y/\partial\hat{y})^T$, and the flux of $\mathbf{q}$ across this edge is the integral of $\mathbf{q}\cdot\mathbf{n}_{\hat{x}}|\mathbf{Y}|$ from 0 to 1, where $\mathbf{n}_{\hat{x}}$ is the unit normal to $\mathbf{Y}$, and $|\mathbf{Y}|$ is the edge Jacobian. Because $\mathbf{n}_{\hat{x}}|\mathbf{Y}| = (\partial y/\partial\hat{y}, -\partial x/\partial\hat{y})^T = \mathbf{e} + \hat{x}\mathbf{f}$, for constant vectors $\mathbf{e}$, $\mathbf{f}$, the flux across the fixed-$\hat{x}$ edge is $\mathbf{q}\cdot\mathbf{e} + \hat{x}\mathbf{q}\cdot\mathbf{f}$, which varies linearly with $\hat{x}$, verifying (P1). The edge Jacobian $|\mathbf{Y}|$ is constant for fixed $\hat{x}$, as is the normal component $\mathbf{q}\cdot\mathbf{n}_{\hat{x}}$, verifying (P2). Thus, in 2-D, the linear flux interpolation Lf_x in (19) is exact for uniform flow.

The 3-D situation is quite different, as shown by the quadratically varying fluxes of uniform flow in (18). A simple example is the "truncated pyramid" hexahedron Q (Figure 3a), whose bottom face at $z = (s_0 - s_1)/2$ ($\hat{z} = 0$) is a square of side s_0 ($-s_0/2 \le x \le s_0/2$, $-s_0/2 \le y \le s_0/2$), and whose top face at $z = (s_1 - s_0)/2$ ($\hat{z} = 1$) is a square of side s_1 ($-s_1/2 \le x \le s_1/2$, $-s_1/2 \le y \le s_0/2$):

$$x \;=\; a(2\hat{x}-1)/2,\; y \;=\; a(2\hat{y}-1)/2,\; z \;=\; (\hat{z}-1/2)(s_1 - s_0), \tag{28}$$

where $a = s_0 + \hat{z}(s_1 - s_0)$. The four lateral faces are planar trapezoids (see Figure 3a). For vertical uniform flow $\mathbf{q} \equiv (0, 0, 1)$, the flux across horizontal interior faces for fixed $\hat{z}$ is the cross-sectional area,

$$f_z(\hat{z}) \;=\; [(1-\hat{z})s_0 + \hat{z}s_1]^2. \tag{29}$$

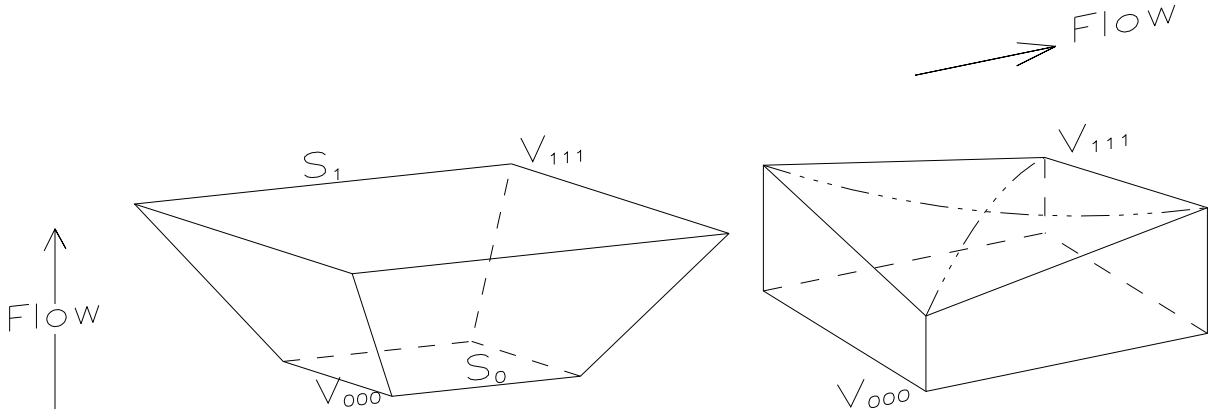

a. Truncated pyramid. b. Tent with curved roof.

Figure 3. **a.** Hexahedral cell in form of a truncated pyramid. Uniform flow parallel to vertical z axis, as indicated by arrow, is assumed. s_0 and s_1 indicate the length of the lower and upper edges, respectively. **b.** Hexahedral cell in form of a tent with curved roof. Uniform flow parallel to horizontal x axis, as indicated by arrow, is assumed. Dash-dot lines show maxima and minima of saddle surface forming cell face $\hat{z} = 1$. For both figures, vertices $\mathbf{v}_{000}$ and $\mathbf{v}_{111}$ are indicated; see Figure 1 for orientation.

A Piola-transformed RT_0 function with the correct top and bottom fluxes has linearly varying flux

$$L f_z(\hat{z}) \;=\; (1-\hat{z})\, f_z(0) + \hat{z}\, f_z(1) = (1-\hat{z})s_0^2 + \hat{z}s_1^2. \tag{30}$$

As (29) and (30) do not agree, Piola-transformed RT_0 functions cannot represent a uniform flow field exactly in 3-D, even on such a simple element. Quadratic flux interpolation (18) treats this case.

Another example is a "tent with curved roof" (Figure 3b) with unit square base at $z = 0$ ($\hat{z} = 0$), vertical lateral faces, height h_0 at two opposite vertices $(0,0,h_0)$, $(1,1,h_0)$, and height h_1 at the other two vertices:

$$x = \hat{x},\; y = \hat{y},\; z = (h_0[(1-\hat{x})(1-\hat{y}) + \hat{x}\hat{y}] + h_1[(1-\hat{x})\hat{y} + \hat{x}(1-\hat{y})])\hat{z}. \tag{31}$$

For horizontal uniform flow $\mathbf{q} \equiv (1,0,0)$, by symmetry the flux across the curved roof F_{z1} at $\hat{z} = 1$ is 0 (this also follows from the divergence theorem). An arbitrary Piola-transformed RT_0 function $\mathbf{v}$ with flux 0 across F_{z1} is a linear combination of the transforms $\boldsymbol{\nu}_{x0}$, $\boldsymbol{\nu}_{x1}$, $\boldsymbol{\nu}_{y0}$, $\boldsymbol{\nu}_{y1}$, $\boldsymbol{\nu}_{z0}$, $\boldsymbol{\nu}_{z1}$ of the six reference basis functions. By (25), the transforms other than $\boldsymbol{\nu}_{z1}$ have vanishing normal component on F_{z1}, pointwise. Thus, the contribution of $\boldsymbol{\nu}_{z1}$ to $\mathbf{v}$ has flux 0 across F_{z1}, so that its coefficient in the linear combination is 0; hence $\mathbf{v}\cdot\mathbf{n}$ vanishes on F_{z1}, pointwise. Since $\mathbf{q}\cdot\mathbf{n} \not\equiv 0$, $\mathbf{q}$ is not a Piola-transformed RT_0 function. More generally, a 3-D shape-function space with (a) degrees of freedom corresponding to face fluxes and (b) pointwise preservation of null normal components across surfaces cannot, for general hexahedra that are trilinear images of a reference cube, contain the constant vector fields. This example points out issues of pointwise velocity interpolation, as opposed to integrated flux interpolation, and the difficulties of treating hexahedra with non-planar faces.

6. VELOCITY INTERPOLATION

Given primary face fluxes $f_{0x}(0)$, etc., and secondary fluxes $f_{2x}(1/2)$, etc., this section determines interpolated velocity approximations at any point $\hat{\mathbf{r}}$ in a cell Q. We build these approximations from components that parallel the covariant vectors $\mathbf{X}$, $\mathbf{Y}$ and $\mathbf{Z}$. For the exact Darcy velocity $\mathbf{q}(\hat{\mathbf{r}})$ these components are designated $\mathbf{q}_\mathbf{X}(\hat{\mathbf{r}})$, $\mathbf{q}_\mathbf{Y}(\hat{\mathbf{r}})$ and $\mathbf{q}_\mathbf{Z}(\hat{\mathbf{r}})$, with

$$\mathbf{q} \;=\; \mathbf{q}_\mathbf{X} + \mathbf{q}_\mathbf{Y} + \mathbf{q}_\mathbf{Z}. \tag{32}$$

The magnitude $U_{\hat{x}}(\hat{\mathbf{r}})$ of the velocity normal to an arbitrary surface at $\hat{x}$, with unit normal $\hat{\mathbf{n}}_x$, is

$$U_{\hat{x}} \;=\; \mathbf{q}\cdot\mathbf{n}_{\hat{x}} \;=\; \mathbf{q}_{\mathbf{X}}\cdot\mathbf{n}_{\hat{x}}, \tag{33}$$

because $\mathbf{n}_{\hat{x}}\cdot\mathbf{q}_{\mathbf{Y}} = \mathbf{n}_{\hat{x}}\cdot\mathbf{q}_{\mathbf{Z}} = 0$. Conversely, if the normal component $U_{\hat{x}}(\hat{x},\hat{y},\hat{z})$ is specified, then

$$\mathbf{q}_{\mathbf{X}}(\hat{x},\hat{y},\hat{z}) = \frac{U_{\hat{x}}(\hat{x},\hat{y},\hat{z})\,|\mathbf{Y}\times\mathbf{Z}|(\hat{x},\hat{y},\hat{z})}{\mathbf{X}(\hat{y},\hat{z})\cdot(\mathbf{Y}\times\mathbf{Z})(\hat{x},\hat{y},\hat{z})}\mathbf{X}(\hat{y},\hat{z}) = U_{\hat{x}}\frac{\mathbf{X}}{J}|\mathbf{Y}\times\mathbf{Z}| \tag{34}$$

satisfies (33). Thus, in theory, a shape function can match an arbitrary $U_{\hat{x}}$, and similarly for $\mathbf{q}_{\mathbf{Y}}$ and $\mathbf{q}_{\mathbf{Z}}$.

Equation (34) is too general; practical shape functions that specify $U_{\hat{x}}(\hat{x},\hat{y},\hat{z})$ must be defined. The relevant unknowns for CVMFE are primary face fluxes $f_{0x}(0)$, $f_{1x}(1)$, $f_{0y}(0)$, $f_{1y}(1)$, $f_{0z}(0)$, $f_{1z}(1)$; hence, $U_{\hat{x}}(\hat{x},\hat{y},\hat{z})$ should depend on $f_{0x}(0)$, $f_{1x}(1)$, and possibly the others. The Piola transformation takes

$$U_{\hat{x}}(\hat{x},\hat{y},\hat{z}) = \frac{(1-\hat{x})\,f_{0x}(0)+\hat{x}\,f_{1x}(1)}{|\mathbf{Y}\times\mathbf{Z}|(\hat{x},\hat{y},\hat{z})} = \frac{L\,f_x(\hat{x})}{|\mathbf{Y}\times\mathbf{Z}|(\hat{x},\hat{y},\hat{z})}, \tag{35}$$

which we verify by checking properties (P1) and (P2). For (P1), as in (14),

$$f_x(\hat{x}) = \int_0^1\int_0^1 U_{\hat{x}}(\hat{x},\hat{y},\hat{z})\,|\mathbf{Y}\times\mathbf{Z}|(\hat{x},\hat{y},\hat{z})\,d\hat{y}\,d\hat{z} = L\,f_x(\hat{x}), \tag{36}$$

and (P2) is immediate. The potential shortcomings of the Piola-transformed shape functions have been noted in previous sections, and we therefore consider alternatives to properties (P1) and (P2).

The fluxes of uniform flow can be matched exactly if we replace (P1) with

(U1) The fluxes $f_x(\hat{x})$, $f_y(\hat{y})$, $f_z(\hat{z})$ vary quadratically with $\hat{x}$, $\hat{y}$, $\hat{z}$, respectively, in the manner of (18).

Here $f_{2x}(1/2)$ must be determined by $f_{0x}(0)$, $f_{1x}(1)$, and possibly the other primary fluxes, in ways to be described later. Because a uniform flow has constant normal component on a planar face, consider also

(U2) The normal components $\mathbf{q}\cdot\mathbf{n}_{\hat{x}}$, $\mathbf{q}\cdot\mathbf{n}_{\hat{y}}$, $\mathbf{q}\cdot\mathbf{n}_{\hat{z}}$ are constant on interior faces with fixed $\hat{x}$, $\hat{y}$, $\hat{z}$, respectively.

For a fixed-$\hat{x}$ interior face, with flux $f_x(\hat{x})$, (U2) requires that

$$U_{\hat{x}}(\hat{x},\hat{y},\hat{z}) = f_x(\hat{x})/A_x(\hat{x}) \tag{37}$$

(unlike (P2), for which $U_{\hat{x}}(\hat{x},\hat{y},\hat{z}) = f_x(\hat{x})/|\mathbf{Y}\times\mathbf{Z}|(\hat{x},\hat{y},\hat{z})$), where A_x is the surface area of the interior face:

$$A_x(\hat{x}) = \int_0^1\int_0^1 |\mathbf{Y}\times\mathbf{Z}|(\hat{x},\hat{y},\hat{z})\,d\hat{y}\,d\hat{z}. \tag{38}$$

Only if the interior face is planar is this straightforward to compute for all $\hat{x}$, making (U2) somewhat impractical. It also matches uniform flow pointwise only under those circumstances. (In general, if the normal direction changes by $O(1)$ across a hexahedral cell of size $O(1)$, as it can, then upon trilinear refinement the direction will change by $O(\Delta x)$ across a refined hexahedron of size $O(\Delta x)$; thus, first-order accuracy in the pointwise representation of uniform flow is the best that one can hope for.) Accordingly, we formulate the less-restrictive property that requires constancy at the ends (primary faces) only:

(UE2) The normal components $\mathbf{q}\cdot\mathbf{n}_{\hat{x}}$, $\mathbf{q}\cdot\mathbf{n}_{\hat{y}}$, $\mathbf{q}\cdot\mathbf{n}_{\hat{z}}$ are constant on the primary cell faces.

Property (UE2) does not specify how normal components vary in the interior; this variation will be a by-product of combinations of (UE2) with the flux variations (P1) and (U1).

A simple modification of the Piola shape functions that suffices to represent uniform flow on the "truncated pyramid" is the replacement of linear with quadratic flux interpolation, combining (U1) with (P2):

$$U_{\hat{x}}(\hat{x},\hat{y},\hat{z}) \;=\; \frac{(1-\hat{x})\,f_{0x}(0)+\hat{x}\,f_{1x}(1)-\hat{x}(1-\hat{x})\,f_{2x}(1/2)}{|\mathbf{Y}\times\mathbf{Z}|(\hat{x},\hat{y},\hat{z})} \;=\; \frac{Q\,f_x(\hat{x})}{|\mathbf{Y}\times\mathbf{Z}|(\hat{x},\hat{y},\hat{z})}. \tag{39}$$

For elements with variable surface Jacobians on primary and/or interior faces, combine (P1) with (UE2):

$$U_{\hat{x}}(\hat{x},\hat{y},\hat{z}) = (1-\hat{x})\frac{f_{0x}(0)}{A_x(0)}\alpha_{0x} + \hat{x}\frac{f_{1x}(1)}{A_x(1)}\alpha_{1x}, \tag{40}$$

where

$$\alpha_{0x} = \frac{|\mathbf{Y}_{0x}\times\mathbf{Z}_{0x}|(\hat{y},\hat{z})}{|\mathbf{Y}\times\mathbf{Z}|(\hat{x},\hat{y},\hat{z})}, \qquad \alpha_{1x} = \frac{|\mathbf{Y}_{1x}\times\mathbf{Z}_{1x}|(\hat{y},\hat{z})}{|\mathbf{Y}\times\mathbf{Z}|(\hat{x},\hat{y},\hat{z})}. \tag{41}$$

At $\hat{x}=0$ and $\hat{x}=1$, (40) reduces to the form of (37), with constant normal component. The interpolated flux is as in (36), which is the reason for the factors α_{0x} and α_{1x} in (40). An analogous development with quadratically varying flux combines (U1) with (UE2) to obtain

$$U_{\hat{x}}(\hat{x},\hat{y},\hat{z}) = (1-\hat{x})\frac{f_{0x}(0)}{A_x(0)}\alpha_{0x} + \hat{x}\frac{f_{1x}(1)}{A_x(1)}\alpha_{1x} - \hat{x}(1-\hat{x})\frac{f_{2x}(1/2)}{A_{2x}}\alpha_{2x}, \tag{42}$$

where α_{2x} and A_{2x} are discussed below. For the secondary surface, two alternatives are suggested for α_{2x}:

$$\alpha_{2x-1} \;=\; \frac{|\mathbf{Y}_{2x}\times\mathbf{Z}_{2x}|}{|\mathbf{Y}\times\mathbf{Z}|}, \qquad \alpha_{2x-2} \;=\; \frac{(\mathbf{Y}_{2x}\times\mathbf{Z}_{2x})\cdot\mathbf{W}_{2x}}{|\mathbf{W}_{2x}|\,|\mathbf{Y}\times\mathbf{Z}|}, \tag{43}$$

where $\mathbf{Y}_{2x}(\hat{z}) = \mathbf{Y}_{1x} - \mathbf{Y}_{0x}$, $\mathbf{Z}_{2x}(\hat{y}) = \mathbf{Z}_{1x} - \mathbf{Z}_{0x}$, and $\mathbf{W}_{2x}$ is defined as

$$\mathbf{W}_{2x} = \int_0^1\int_0^1 (\mathbf{Y}_{2x}(\hat{z})\times\mathbf{Z}_{2x}(\hat{y}))\,d\hat{y}d\hat{z} \;=\; \int_0^1 \mathbf{Y}_{2x}(\hat{z})\,d\hat{z} \times \int_0^1 \mathbf{Z}_{2x}(\hat{y})\,d\hat{y} \;=\; \mathbf{Y}_{2x}(1/2)\times\mathbf{Z}_{2x}(1/2). \tag{44}$$

To show the second equality in (44), write out each component of the cross product in the vector double integral, observe that the terms in the resulting scalar double integrals can be factored into scalar single integrals, and finally reassemble these into the components of a cross product of vector single integrals. The last equality follows from the linearity of $\mathbf{Y}_{2x}$ and $\mathbf{Z}_{2x}$ with respect to $\hat{z}$ and $\hat{y}$, respectively. Related to these two alternatives are two alternative definitions for the area A_{2x} of the secondary surface:

$$A_{2x-1} \;=\; \int_0^1\int_0^1 |\mathbf{Y}_{2x}\times\mathbf{Z}_{2x}|\,d\hat{y}d\hat{z}, \qquad A_{2x-2} \;=\; \int_0^1\int_0^1 (\mathbf{Y}_{2x}\times\mathbf{Z}_{2x})\cdot\frac{\mathbf{W}_{2x}}{|\mathbf{W}_{2x}|}\,d\hat{y}d\hat{z} \;=\; |\mathbf{W}_{2x}|. \tag{45}$$

Both expressions in (43) are approximate for non-planar secondary faces. For twisted planar secondary faces, A_{2x-1} is incorrect because it is based on a mapping for a convex region and prevents cancellation of opposite directions in $\mathbf{Y}_{2x}\times\mathbf{Z}_{2x}$; A_{2x-2} is correct in this case, and α_{2x-2} should be superior to α_{2x-1} as the twisted-face differential area is used in the construction of this ratio. For planar, non-twisted, secondary faces, $(\mathbf{Y}_{2x}\times\mathbf{Z}_{2x})(\hat{y},\hat{z})$ is a positive multiple of $\mathbf{W}_{2x}$, so that both forms in (43) and (45) produce identical results.

For the velocity magnitude, though other forms have been studied, we have found that (42) performs well because the ratios (41) and (43) adjust the magnitude by comparing a differential element on the interior surface with one on the cell surface. In contrast to $U_{\hat{x}}(\hat{x},\hat{y},\hat{z})$ of (33), the approximate velocity magnitudes in (40) and (42) become constant on the cell faces at $\hat{x}=0$ and $\hat{x}=1$. This results because (40) and (42) are based on the flux interpolation functions (19) and (18), respectively; these interpolation functions assume bulk fluxes at the cell faces to approximate the bulk flux on a congruent interior face. This level of approximation is consistent with the discrete continuity and Darcy equations, (9) and (13).

Use $U_{\hat{x}}$ from (42) to approximate (34); then the approximation $\mathbf{V}_{\mathbf{X}}$ of $\mathbf{q}_{\mathbf{X}}$ in (34) is

$$\mathbf{V}_{\mathbf{X}} \;=\; \frac{\mathbf{X}}{J}[(1-\hat{x})\,\beta_{x0}\,f_{x0} + \hat{x}\,\beta_{x1}\,f_{x1} - \hat{x}(1-\hat{x})\,\beta_{x2}\,f_{x2}], \tag{46}$$

where $f_{x0} = f_{0x}(0)$ and $f_{x1} = f_{1x}(1)$ are the actual fluxes across cell faces $\hat{x}=0$ and $\hat{x}=1$, and f_{x2} is the secondary flux to be determined later. The ratios β_{x0} and β_{x1} and the suggested alternatives for β_{x2} are

$$\beta_{x0} \;=\; \left|\frac{\mathbf{Y}\times\mathbf{Z}}{A_x}\right|_{\hat{x}=0}, \quad \beta_{x1} \;=\; \left|\frac{\mathbf{Y}\times\mathbf{Z}}{A_x}\right|_{\hat{x}=1}, \quad \beta_{x2-1} \;=\; \frac{|\mathbf{Y}_{2x}\times\mathbf{Z}_{2x}|}{A_{2x-1}}, \quad \beta_{x2-2} \;=\; \frac{(\mathbf{Y}_{2x}\times\mathbf{Z}_{2x})\cdot\mathbf{W}_{2x}}{|\mathbf{W}_{2x}|^2}. \tag{47}$$

Similar expressions can be derived for interpolation functions in the **Y** and **Z** directions:

$$\mathbf{V_Y} \;=\; \frac{\mathbf{Y}}{J}[(1-\hat{y})\,\beta_{y0}\,f_{y0}+\hat{y}\,\beta_{y1}\,f_{y1}-\hat{y}(1-\hat{y})\,\beta_{y2}\,f_{y2}], \tag{48}$$

$$\mathbf{V_Z} \;=\; \frac{\mathbf{Z}}{J}[(1-\hat{z})\,\beta_{z0}\,f_{z0}+\hat{z}\,\beta_{z1}\,f_{z1}-\hat{z}(1-\hat{z})\,\beta_{z2}\,f_{z2}], \tag{49}$$

where

$$\beta_{y0} \;=\; \left|\frac{\mathbf{Z}\times\mathbf{X}}{A_y}\right|_{\hat{y}=0}, \qquad \beta_{y1} \;=\; \left|\frac{\mathbf{Z}\times\mathbf{X}}{A_y}\right|_{\hat{y}=1}, \qquad \beta_{z0} \;=\; \left|\frac{\mathbf{X}\times\mathbf{Y}}{A_z}\right|_{\hat{z}=0}, \qquad \beta_{z1} \;=\; \left|\frac{\mathbf{X}\times\mathbf{Y}}{A_z}\right|_{\hat{z}=1},$$

$$\beta_{y2-1} \;=\; \frac{|\mathbf{Z}_{2y}\times\mathbf{X}_{2y}|}{A_{2y-1}}, \qquad \beta_{y2-2} \;=\; \frac{(\mathbf{Z}_{2y}\times\mathbf{X}_{2y})\cdot\mathbf{W}_{2y}}{|\mathbf{W}_{2y}|^2},$$
$$\beta_{z2-1} \;=\; \frac{|\mathbf{X}_{2z}\times\mathbf{Y}_{2z}|}{A_{2z-1}}, \qquad \beta_{z2-2} \;=\; \frac{(\mathbf{X}_{2z}\times\mathbf{Y}_{2x})\cdot\mathbf{W}_{2z}}{|\mathbf{W}_{2z}|^2.}$$

The associated secondary vectors are $\mathbf{X}_{2y}=\mathbf{X}|_{\hat{y}=1}-\mathbf{X}|_{\hat{y}=0}$, $\mathbf{Z}_{2y}=\mathbf{Z}|_{\hat{y}=1}-\mathbf{Z}|_{\hat{y}=0}$, $\mathbf{X}_{2z}=\mathbf{X}|_{\hat{z}=1}-\mathbf{X}|_{\hat{z}=0}$ and $\mathbf{Y}_{2z}=\mathbf{Y}|_{\hat{z}=1}-\mathbf{Y}|_{\hat{z}=0}$; f_{y0}, f_{y1}, f_{z0} and f_{z1} are fluxes across cell faces at $\hat{y}=0$, $\hat{y}=1$, $\hat{z}=0$ and $\hat{z}=1$; and f_{y2} and f_{z2} are fluxes associated with the secondary faces in the logical y and z directions. Areas $A_y(\hat{y})$ and $A_z(\hat{z})$ are similar to (38) and secondary areas A_{2y-1} and A_{2z-1} are similar to A_{2x-1} in (45).

The cell approximation $\mathbf{V}_c$ of the velocity $\mathbf{q}$ can be obtained from these relations as

$$\mathbf{V}_c \;=\; \mathbf{V_X}+\mathbf{V_Y}+\mathbf{V_Z}. \tag{50}$$

For uniform flow, where (18) is exact, $\mathbf{V}_c$ can equal $\mathbf{q}$ provided that all cell faces are planar; however, because of possible errors in the velocity magnitude correction ratios β_{x2}, β_{y2} and β_{z2} for the secondary face, this equality may not hold. This discrepancy will be discussed further subsequently.

7. VELOCITY SHAPE FUNCTIONS

This section finalizes the shape functions by developing accurate approximations for the secondary fluxes f_{x2}, f_{y2} and f_{z2} in terms of the primary fluxes f_{x0}, f_{x1}, f_{y0}, f_{y1}, f_{z0} and f_{z1}. The exact relation for f_{x2} is (17c) with $\hat{x}=1/2$; one could propose (50) to approximate $\mathbf{q}$ in (17c), except that $\mathbf{V}_c$ itself requires knowledge of f_{x2}, f_{y2} and f_{z2}. We propose, instead, to approximate $\mathbf{q}$ in (17c) with a bulk value $\langle\mathbf{q}\rangle$ for the cell Q. The approximation $\tilde{f}_{x2}$ for the secondary flux f_{x2} would then be

$$\tilde{f}_{x2} \;=\; \langle\mathbf{q}\rangle\cdot\int_0^1\int_0^1(\mathbf{Y}_{2x}\times\mathbf{Z}_{2x})\,d\hat{y}d\hat{z} \;=\; \langle\mathbf{q}\rangle\cdot\mathbf{W}_{2x}, \tag{51}$$

where $\mathbf{W}_{2x}$, derived in (44), is a bulk equivalent of $\mathbf{Y}_{2x}\times\mathbf{Z}_{2x}$ that also appears in (43) and (45) to correct for twisted planar secondary faces. The fact that $|\mathbf{W}_{2x}|$ gives the correct area for a twisted planar secondary face inspired the differential area used in these expressions. For the bulk cell velocity $\langle\mathbf{q}\rangle$, we propose:

$$\begin{aligned}\langle\mathbf{q}\rangle \;=\; & \frac{1}{8}[\mathbf{V}_c(0,0,0)+\mathbf{V}_c(1,0,0)+\mathbf{V}_c(0,1,0)+\mathbf{V}_c(0,0,1)\\ & +\;\mathbf{V}_c(1,1,1)+\mathbf{V}_c(0,1,1)+\mathbf{V}_c(1,0,1)+\mathbf{V}_c(1,1,0)].\end{aligned} \tag{52}$$

That is, the cell velocity $\mathbf{V}_c$ at the corners is averaged. At the corners, the secondary fluxes are not needed in $\mathbf{V}_c$, so that we can write

$$\mathbf{V}_c(i,j,k) \;=\; [\,f_{xi}\,\mathbf{X}(j,k)\,\beta_{xi}(j,k)+f_{yj}\,\mathbf{Y}(i,k)\,\beta_{yj}(i,k)+f_{zk}\,\mathbf{Z}(i,j)\,\beta_{zk}(i,j)]\big/J(i,j,k), \tag{53}$$

where $i = 0,1$; $j = 0,1$; $k = 0,1$. With (51), (52) should produce a reasonable estimate of the secondary flux, f_{x2}; for uniform flow, it is exact. Appendix D shows that, for a general smooth velocity field $\mathbf{q}$, this approximation preserves the second-order accuracy of the quadratic flux interpolation Qf_x, as in (22).

This shows that f_{x2} can be approximated as a linear combination of the primary fluxes f_{x0}, f_{x1}, f_{y0}, f_{y1}, f_{z0} and f_{z1}, and similarly for f_{y2} and f_{z2}. The general secondary-flux approximation is, for $\kappa = x$, y, or z, and $l = 0,1$:

$$\tilde{f}_{\kappa 2} \;=\; r_{\kappa x0} f_{x0} + r_{\kappa x1} f_{x1} + r_{\kappa y0} f_{y0} + r_{\kappa y1} f_{y1} + r_{\kappa z0} f_{z0} + r_{\kappa z1} f_{z1}, \tag{54}$$

$$r_{\kappa xl} \;=\; \frac{\mathbf{W}_{2\kappa}}{8} \cdot \sum_{m=0}^{1} \sum_{p=0}^{1} \frac{\beta_{xl}(m,p)\mathbf{X}(m,p)}{J(l,m,p)}, \tag{55a}$$

$$r_{\kappa yl} \;=\; \frac{\mathbf{W}_{2\kappa}}{8} \cdot \sum_{m=0}^{1} \sum_{p=0}^{1} \frac{\beta_{yl}(m,p)\mathbf{Y}(m,p)}{J(m,l,p)}, \tag{55b}$$

$$r_{\kappa zl} \;=\; \frac{\mathbf{W}_{2\kappa}}{8} \cdot \sum_{m=0}^{1} \sum_{p=0}^{1} \frac{\beta_{zl}(m,p)\mathbf{Z}(m,p)}{J(m,p,l)}. \tag{55c}$$

Here, $J(\hat{x},\hat{y},\hat{z})$ is the Jacobian in (5) and β_{xl}, β_{yl} and β_{zl} are as in (46)–(49). Equation (54) follows by substituting (53) into (52) and (52) into (51). Following (44), the bulk vectors $\mathbf{W}_{2y}$ and $\mathbf{W}_{2z}$ are

$$\mathbf{W}_{2y} = \int_0^1 \int_0^1 (\mathbf{Z}_{2y}(\hat{x}) \times \mathbf{X}_{2y}(\hat{z}))\, d\hat{x}d\hat{z} = \mathbf{Z}_{2y}(1/2) \times \mathbf{X}_{2y}(1/2)\,, \tag{56a}$$

$$\mathbf{W}_{2z} = \int_0^1 \int_0^1 (\mathbf{X}_{2z}(\hat{y}) \times \mathbf{Y}_{2z}(\hat{x}))\, d\hat{x}d\hat{y} = \mathbf{X}_{2z}(1/2) \times \mathbf{Y}_{2z}(1/2)\,. \tag{56b}$$

These forms complete the velocity interpolation functions $\mathbf{V}_\mathbf{X}$, $\mathbf{V}_\mathbf{Y}$ and $\mathbf{V}_\mathbf{Z}$ in (46)–(49).

Now shape functions can be obtained directly from (50) by collecting coefficients of f_{x0}, f_{x1}, f_{y0}, f_{y1}, f_{z0} and f_{z1}. In terms of shape functions $\boldsymbol{\nu}_{x0}$, $\boldsymbol{\nu}_{x1}$, $\boldsymbol{\nu}_{y0}$, $\boldsymbol{\nu}_{y1}$, $\boldsymbol{\nu}_{z0}$ and $\boldsymbol{\nu}_{z1}$, the cell velocity becomes

$$\mathbf{V}_c \;=\; f_{x0}\boldsymbol{\nu}_{x0} + f_{x1}\boldsymbol{\nu}_{x1} + f_{y0}\boldsymbol{\nu}_{y0} + f_{y1}\boldsymbol{\nu}_{y1} + f_{z0}\boldsymbol{\nu}_{z0} + f_{z1}\boldsymbol{\nu}_{z1}, \tag{57}$$

where

$$\boldsymbol{\nu}_{x0} \;=\; \frac{1}{J}[(1-\hat{x})\mathbf{X}\beta_{x0} - \hat{x}(1-\hat{x})\,\mathbf{X}\beta_{x2}r_{xx0} - \hat{y}(1-\hat{y})\,\mathbf{Y}\beta_{y2}r_{yx0} - \hat{z}(1-\hat{z})\,\mathbf{Z}\beta_{z2}r_{zx0}], \tag{58a}$$

$$\boldsymbol{\nu}_{x1} \;=\; \frac{1}{J}[\hat{x}\mathbf{X}\beta_{x1} - \hat{x}(1-\hat{x})\,\mathbf{X}\beta_{x2}r_{xx1} - \hat{y}(1-\hat{y})\,\mathbf{Y}\beta_{y2}r_{yx1} - \hat{z}(1-\hat{z})\,\mathbf{Z}\beta_{z2}r_{zx1}], \tag{58b}$$

$$\boldsymbol{\nu}_{y0} \;=\; \frac{1}{J}[(1-\hat{y})\mathbf{Y}\beta_{y0} - \hat{x}(1-\hat{x})\,\mathbf{X}\beta_{x2}r_{xy0} - \hat{y}(1-\hat{y})\,\mathbf{Y}\beta_{y2}r_{yy0} - \hat{z}(1-\hat{z})\,\mathbf{Z}\beta_{z2}r_{zy0}], \tag{58c}$$

$$\boldsymbol{\nu}_{y1} \;=\; \frac{1}{J}[\hat{y}\mathbf{Y}\beta_{y1} - \hat{x}(1-\hat{x})\,\mathbf{X}\beta_{x2}r_{xy1} - \hat{y}(1-\hat{y})\,\mathbf{Y}\beta_{y2}r_{yy1} - \hat{z}(1-\hat{z})\,\mathbf{Z}\beta_{z2}r_{zy1}], \tag{58d}$$

$$\boldsymbol{\nu}_{z0} \;=\; \frac{1}{J}[(1-\hat{z})\mathbf{Z}\beta_{z0} - \hat{x}(1-\hat{x})\,\mathbf{X}\beta_{x2}r_{xz0} - \hat{y}(1-\hat{y})\,\mathbf{Y}\beta_{y2}r_{yz0} - \hat{z}(1-\hat{z})\,\mathbf{Z}\beta_{z2}r_{zz0}], \tag{58e}$$

$$\boldsymbol{\nu}_{z1} \;=\; \frac{1}{J}[\hat{z}\mathbf{Z}\beta_{z1} - \hat{x}(1-\hat{x})\,\mathbf{X}\beta_{x2}r_{xz1} - \hat{y}(1-\hat{y})\,\mathbf{Y}\beta_{y2}r_{yz1} - \hat{z}(1-\hat{z})\,\mathbf{Z}\beta_{z2}r_{zz1}]. \tag{58f}$$

Properly reconfigured, $\mathbf{V}_c$ from adjoining cells approximate $\mathbf{V}_{i+1/2,j,k}$ of (12). For a cell $Q_{i,j,k}$, the shape functions are as in (8) and comply with property (10); that is, a discrete continuity equation is formulated for $Q_{i,j,k}$. This completes the CVMFE method. Note that if normal components were approximated with linear forms such as (40) instead of (42), then only the first term in each of (58a)–(58f) would remain (also see

reference [4]). Because of the complexity of the shape functions and the test function (11), the integrations in (13) were calculated with a very precise quadrature; the effect of quadrature will be investigated in the future. The resulting algebraic equations were solved with the Schur complement to decouple the flux equations from the pressure equations, followed by a variant of the iterative scheme of [11].

The shape functions for 3-D hexahedral cells can have a quadratic dependence when the secondary fluxes are nonzero. This condition occurs whenever a cell has non-parallel opposite faces; only regular meshes or irregular meshes with a 2-D aspect will retain strictly linear shape functions. For uniform flow, these shape functions can give exact velocity results if the hexahedral cell has planar primary (exterior) and secondary faces. Mesh construction can usually produce planar primary faces, but planar secondary faces can be more problematic, and the distortion on the secondary faces can be rather severe. In particular, secondary faces can be non-planar even when all exterior faces are planar. Planar secondary faces can be forced by insisting that each cell have at least one pair of parallel opposite faces; however, these secondary faces may be twisted as well as planar.

8. UNIFORM FLOW TESTS

Uniform flow should be approximated accurately in any numerical simulation of flow through porous media, and CVMFE usually does so. However, accuracy can be lost in certain cases of irregular cells, particularly if either the primary or secondary cell faces are non-planar. Consider non-planar primary, exterior faces. Two of the three covariant vectors are tangent to every exterior face, and the velocity shape functions depend on these vectors, so that approximate velocities near non-planar faces should be curved along with these faces, deviating from a uniform flow field. The "tent with curved roof" in Section 5 is an example. For secondary faces, the reasoning is less clear but likely similar.

The error between simulations and exact, uniform flow is measured with the L^2 norm

$$L^2 \;=\; \left\{ \sum_i Q_i^* \left[(\tilde{f}_i - f_i)/A_i \right]^2 \Big/ \sum_i Q_i^* \right\}^{1/2}, \tag{59}$$

where, for all faces $F_i \in \Omega$, $\tilde{f}_i$ and f_i are the estimated and true fluxes, A_i is the area, and Q_i^* is the control volume straddling F_i. The numerator of (59) is a discrete volume integral of the square of the velocity error, and the denominator normalizes the error to be independent of the domain volume. In the test problems with a dominant linear flow direction, the mean velocity will be 1; in the next section, for a non-uniform flow test with corner-to-corner flow, it will be of order 1. Thus, the reported L^2 norms can be regarded as relative errors and can be compared from one test to another.

Three different coarse meshes were used in the uniform flow tests: in tests 1 and 2, cells were quasi-random with planar primary faces, while the vertices of test 3 were random and all interior primary cell faces were non-planar. The domain Ω was a regular cube in all cases with $4\times4\times4$ coarse mesh. Each discretization was refined smoothly through three levels. At each level, each cell was divided into eight subcells, halving it in the reference cube in each direction. This yielded refined meshes of $8\times8\times8$, $16\times16\times16$ and $32\times32\times32$.

In test 1, irregular cells with planar, quasi-random faces were generated, starting with random vertices on three adjoining exterior faces of Ω. These vertices were created from a regular mesh on each face by multiplying each regular vertex location by a random number close to one. Starting at the corner where the three exterior faces meet, cells were created by connecting vertices of three existing cell faces to an interior vertex, requiring that the new cell faces forming this connection be planar. This results in interior cells with planar, quasi-random primary faces. The secondary faces of cells in this grid are rarely, if ever, planar. In test 2, the random vertices on the three adjoining exterior faces of Ω were required to fall on parallel grid lines perpendicular to the x direction (Figure 4). This affects primarily the x cell faces, which are all parallel and follow the grid lines perpendicular to the x direction. The y and z cell faces remain quasi-random after the inward projection procedure, but are constrained in sharing vertices with the x faces. The chief difference

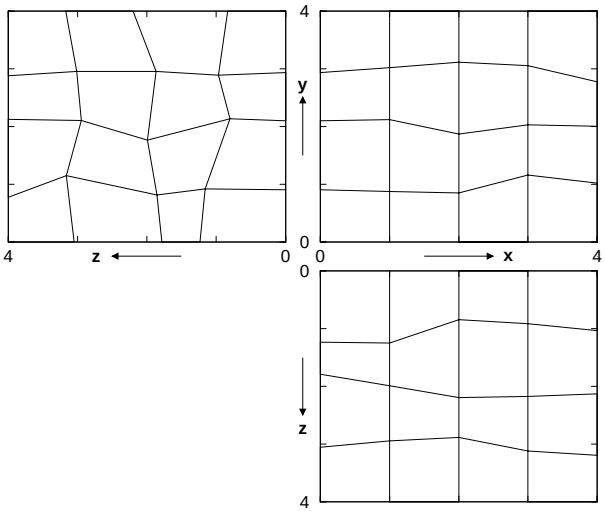

Figure 4. Three exterior faces of the test 2 domain that share vertex (0,0,0). Fold up the left (*yz*) face along the *y*-axis and the bottom (*xz*) face along the *x*-axis.

between the two types of grids is that the secondary faces of cells in the test 2 grid are always planar but occasionally twisted. The coarse mesh for test 3 was created by randomly perturbing the vertex locations of a regular, $4\times4\times4$ grid; the vertices on $\partial\Omega$ were perturbed only within the plane forming the surface. None of the interior cell faces were planar. The random perturbation was limited to a maximum of 5% of the unperturbed cell dimension; this small amount of grid distortion may easily be expected in flow simulations.

In test 1, where all *x*, *y* and *z* are quasi-random, the uniform flow $\mathbf{q} = (1,0,0)$ was imposed via homogeneous $\mathbf{K}$ and appropriate flux boundary conditions. It is then simple to calculate the exact fluxes across the interior faces of the discretization. In test 2, with quasi-random *y* and *z* faces, similar flux conditions were imposed to obtain $\mathbf{q} = (1,0,0)$ and (in a separate calculation) $\mathbf{q} = (0,1,0)$. These two different flux conditions were used because, on the average, the test 2 mesh is anisotropic. The uniform flow in test 3 was diagonal across the mesh, from cell Q_{111} to cell Q_{444}. Results from the non-linear velocity shape functions (sf1, sf2) developed herein are compared with linear velocity shape functions (sf0); explicit forms for sf0 can be found in [4]. Here sf1 and sf2 refer to secondary-flux correction factors β_{x2-1}, β_{y2-1}, β_{z2-1} and β_{x2-2}, β_{y2-2}, β_{z2-2}, respectively, in (46). The L^2 norm results are in Table I.

For test 1, the non-linear shape functions (sf1, sf2) are superior to the linear ones (sf0) over the entire range of mesh refinement ($1\times$–$8\times$) by one to two orders of magnitude. Thus, the quadratic flux interpolation (18) has a substantial impact on the second-order error in velocity interpolation, particularly on coarse grids, which are important in practice. For the non-linear shape functions, there is little difference between the two correction factors, and results become identical as the mesh is refined. For either sf1 or sf2, the L^2 norms are not large in any case; this probably reflects the moderate degree of distortion contained in the mesh. With the first and subsequent refinements, the cell faces become slightly non-planar, adding some error to the solution. This may explain the slightly smaller reduction factors for the first refinement. Subsequent refinements reduce the L^2 norm by a factor of 3.3 to 3.7, as the effect of non-planarity decreases. The reduction factors for sf0 are 5 to 5.5; as the secondary flux becomes less important with refinement, the cells become closer to parallelepipeds, and sf0 L^2 norms come closer to those of sf1 and sf2.

For test 2, with parallel faces in the *x* direction and flow in the *x* direction (*x* fd), the L^2 norm results for the coarse grid ($1\times$) are two orders of magnitude greater for sf0 than for sf1. However, after three mesh refinements ($8\times$), the ratio between sf0 and sf1 is only a factor of three; the more rapid reduction of this ratio here, relative to the test 1 case, probably reflects the strongly diminished importance of the secondary flux with mesh refinement. For x fd, the non-linear shape functions sf1 and sf2 give very different results on the coarse grid ($1\times$); sf2 reflects an exact solution. This does not occur for sf1 because the random grid, in this case, produces planar *x*-direction secondary faces, some of which are twisted. While the sf2 correction

Table I. L^2 norm results for uniform flow tests. Test 1: all cell faces random and planar; flow in x direction. Test 2: cell faces y and z random; x faces parallel; all cell faces planar. Test 3: all vertices random; all internal faces non-planar; diagonal flow. sf0: linear shape function [4]. sf1: non-linear shape function using first secondary flux correction factors β_{x2-1}, etc. sf2: same with β_{x2-2}, etc. fd: flow direction. *: $< 10^{-10}$

test		grid refinement, $L2$ norm			
no	case	1×	2×	4×	8×
1	sf0	3.591×10^{-04}	7.103×10^{-05}	1.286×10^{-05}	2.344×10^{-06}
	sf1	6.098×10^{-06}	2.111×10^{-06}	6.453×10^{-07}	1.737×10^{-07}
	sf2	6.116×10^{-06}	2.111×10^{-06}	6.452×10^{-07}	1.737×10^{-07}
2	sf0, x fd	1.817×10^{-03}	3.176×10^{-04}	5.777×10^{-05}	1.070×10^{-05}
	sf1, x fd	1.862×10^{-05}	3.608×10^{-05}	1.202×10^{-05}	3.311×10^{-06}
	sf2, x fd	exact*	3.599×10^{-05}	1.202×10^{-05}	3.311×10^{-06}
	sf0, sf1, sf2, y fd	exact*	1.666×10^{-05}	5.210×10^{-06}	1.401×10^{-06}
3	sf0	1.232×10^{-04}	4.045×10^{-05}	1.151×10^{-05}	3.199×10^{-06}
	sf1	1.039×10^{-04}	3.940×10^{-05}	1.137×10^{-05}	3.182×10^{-06}
	sf2	1.038×10^{-04}	3.940×10^{-05}	1.137×10^{-05}	3.182×10^{-06}

factors can compensate completely for twisted planar faces, the sf1 correction factors cannot. Both non-linear shape functions produce nearly identical L^2 norms with the first refinement (2×) of the mesh, and both degrade relative to the initial mesh (1×). This is likely due to the introduction of non-planar primary faces in the 2× refined mesh. With refinement, the tendency for a planar secondary face to be twisted is reduced, and the L^2 norms for sf1 and sf2 become identical. For both sf1 and sf2, the second refinement (4×) produces a reduction in the L^2 norm of about 3; with the third (8×), it increases to 3.6. The reduction factor for sf0 is about 5 for all refinements.

The y flow direction results for test 2 are essentially identical for all three shape functions (sf0, sf1 and sf2); this is because the secondary faces are oriented such that they can be influenced only by flow in the x direction, regardless of refinement. To see this, note that by (44), (56a), and (56b), $\mathbf{W}_{2x} = \mathbf{Y}_{2x}(1/2) \times \mathbf{Z}_{2x}(1/2)$, with analogous expressions for $\mathbf{W}_{2y}$ and $\mathbf{W}_{2z}$; the $\mathbf{X}_2 = \mathbf{X}_1 - \mathbf{X}_0$ vectors are differences of vectors that have the same x-component, which is equal to the distance between the parallel planes normal to the x-axis, hence the $\mathbf{X}_2$ vectors lie in these planes. The $\mathbf{Y}_2$ and $\mathbf{Z}_2$ vectors also lie in these planes; hence, all cross products in the $\mathbf{W}_2$ vectors are parallel to the x-axis. Thus, the fluxes f_{x2} for the secondary faces are null for for either sf1 or sf2; as sf0 does not include the effects of a secondary flux term, all three results are identical. For all three, the solution degrades with the first refinement (2×), and subsequent refinements improve the L^2 norm by a factor of 3.3 to 3.7. The initial degradation in the L^2 norm is likely caused by non-planar primary cell faces in the refined mesh.

Test 3 examined the effect of non-planar faces, in a realistic scenario of mesh distortion, on the L^2 norm; an exact solution is not expected under these circumstances. The 2-D mesh-face distortion can be measured by the sine of the angle between poles located at opposite vertices of a face; the average sine of the largest angle between poles was 0.03 for the initial mesh (1×). Table I indicates that the flow field is fairly well resolved for the initial mesh, regardless of the shape function used; sf1 and sf2 are only marginally better than sf0. Compared to test 1, it is apparent that even the small amount of facial distortion in this mesh degrades the solution, masking most of the corrective effect of the quadratic term in sf1 and sf2. With refinement (8×), the average sine of the largest angle on the non-planar surfaces decreased to 0.003; the

Table II. L^2 norm results for non-uniform flow tests. Test 1: homogeneous medium; corner-to-corner flow. Test 1e: repeat of L^2 norm calculation for test 1 with exclusion zone around flux boundary conditions. Test 2: heterogeneous medium. reg: orthogonal, regular mesh. sf1: shape function using first secondary flux correction factor in conjunction with the quasi-random mesh. sf2: shape function using second secondary flux correction factor in conjunction with the quasi-random mesh.

test		grid refinement, $L2$ norm		
no	case	$1\times$	$2\times$	$4\times$
1	reg	1.504×10^{-3}	6.593×10^{-4}	3.436×10^{-4}
	sf1, sf2	1.658×10^{-3}	7.117×10^{-4}	3.704×10^{-4}
1e	reg	1.109×10^{-3}	2.407×10^{-4}	4.638×10^{-5}
	sf1, sf2	1.114×10^{-3}	2.478×10^{-4}	4.766×10^{-5}
2	reg	2.371×10^{-2}	1.424×10^{-2}	6.922×10^{-3}
	sf1, sf2	2.489×10^{-2}	1.473×10^{-2}	7.086×10^{-3}

decrease was uniform and first-order. Concomitant with this decrease, the reduction factor for the L^2 norm increased from 2.6 to 3.6. As expected, differences between results from sf0, sf1 and sf2 dissipate as the role of the secondary flux dissipates with grid refinement.

9. NON-UNIFORM FLOW TESTS

In this section, second-order behavior of the flux truncation error (22) is examined, as well as non-uniform flow in heterogeneous media. For all tests, a regular and a quasi-random discretization were used; for the quasi-random discretization, all *x*, *y* and *z* cell faces were randomized with the test 1 procedure described in the previous section. Initial grids, before refinement, were $5\times5\times5$; the domain Ω was a regular cube. For the quasi-random meshes, non-linear shape functions with both types of correction factors, sf1 and sf2, were tested.

In test 1, with homogeneous **K**, non-uniform corner-to-corner flow was obtained by injecting a unit flux on the three exterior faces of cell $(1,1,1)$ and extracting a unit flux from those of cell $(5,5,5)$. With refinement of the mesh, the flux boundary conditions were maintained, preserving the original facial area of the applied fluxes. In test 2, a heterogeneous hydraulic conductivity field was generated for a central part of the $5\times5\times5$ cell mesh, occupying $3\times5\times5$ cells of the mesh. With a mean value of about 100, **K** ranged over three orders of magnitude (although a range of two orders was most common). The $1\times5\times5$ groups of cells at each end of the heterogeneous zone were assigned a uniform **K** of 100; uniform flux boundary conditions were applied over the exterior faces of these cells to create a mean flow in the *x*-direction. Grid refinement preserved the structure of **K**. In these simulations, the finest $(40\times40\times40)$ discretization was assumed to represent the "true" solution; L^2 norms, as defined in (59), were obtained by comparing coarser discretizations with the finest. Intermediate discretizations were $10\times10\times10$ and $20\times20\times20$. The L^2 norm results for these simulations are summarized in Table II.

Note that the errors are generally greater than those of Table I; this likely reflects the non-uniformity of the flow rather than shape-function issues. That Table II shows the same results for sf1 and sf2 indicates that any difference between them is overshadowed by the errors due to non-uniform flow. It is encouraging that the irregular-mesh L^2 norms are about the same as for the regular mesh, especially for the unrefined case, though it is not clear which aspects of the treatment of mesh distortion are responsible for this.

For non-uniform flow in a homogeneous medium (test 1), the L^2 norm decreases with each mesh refinement by a factor of about two, indicating first-order convergence. Though (22) is second-order, [1] demonstrates that convergence will be degraded if there are singularities in the exact solution. Flux boundary conditions on parts of the faces of $\partial\Omega$ cause singularities at the points where the nonzero fluxes meet no-flow conditions. In test 1e, the L^2 norm estimate (59) was modified to exclude errors from a zone surrounding each of the flux boundary conditions; then the L^2 norm decreases with mesh refinement by factors varying from 4.5 to 5.2, in line with the second-order convergence expected from (22). For the heterogeneous case (test 2), the L^2 norm results produce rates of improvement which vary from 1.7 to 2.5 with mesh refinement, suggesting first-order convergence. For a heterogeneous problem with many internal discontinuities in $\mathbf{K}$, this is expected, as these discontinuities can result in singularities in the exact solution [1].

10. CONCLUDING REMARKS

The most general conclusion of this investigation is that, for distorted logically rectangular meshes, the lowest-order velocity shape functions should not vary linearly with space, in terms of either the velocity or the flux. This results from a study of flux conservation in a general, hexahedral cell, where a quadratic term is needed in order to match the flux of uniform flow; this is demonstrated with (18), and the second-order estimate of the error of quadratic flux interpolation is given by (22). In particular, the linearly varying flux of the Piola transformation cannot match uniform flow on general hexahedral cells.

This quadratic term, however, leads to an additional unknown secondary flux, f_{x2}, which must be independently estimated. The method in (51)–(52) for this estimate is exact for uniform flow; in general, it is at least concordant with the second-order flux approximation (18), as demonstrated in Appendix D. In addition, we have found that weightings for (42) such as (41) and (43), which adjust the velocity magnitude by comparing a differential element in the interior with a differential element on the cell face, work well to interpolate the velocity magnitude to the interior.

Meshes with non-planar primary and secondary cell faces will lead to some degradation in accuracy. Uniform flow tests suggest that, as long as this type of cell distortion is kept minimal, overall accuracy is not greatly affected. In particular, the L^2 flux error for a mesh containing rather smooth non-planar secondary faces was not excessive. Indeed, if at least two faces of every cell can be made parallel, then shape functions which compensate for twisted planar faces can apparently eliminate this error. The cost is the loss of generality in instituting an irregular grid. Second-order convergence was strongly indicated by the reduction factors for the L^2 norms for all the uniform flow tests.

In regions away from points of discontinuity, the non-uniform flow simulations in a homogeneous medium also show second-order convergence. First-order convergence is seen in non-uniform flow simulations in heterogeneous media. Overall convergence of most practical simulations, which will have singularities or points of discontinuity, should be first-order.

The results reported here do not include non-smooth "random" refinements, in which angular deviations do not decrease (see discussion after (23)). Preliminary computations show the expected first-order convergence in many cases, and less in some others, possibly due to severe distortions caused by the constrained procedure that generated the refined meshes. More thorough investigations of random refinements will be reported in the future.

11. APPENDIX A

A form, explicit in $\hat{x}$, for the logical x direction cross product $\mathbf{Y} \times \mathbf{Z}$, is derived; the logical y and z direction cross products are similar. From (4) and definitions of the covariant vectors,

$$\mathbf{Y} \;=\; (1-\hat{x})\mathbf{Y}_{0x} + \hat{x}\mathbf{Y}_{1x}, \qquad \mathbf{Z} \;=\; (1-\hat{x})\mathbf{Z}_{0x} + \hat{x}\mathbf{Z}_{1x}, \tag{60}$$

where $\mathbf{Y}_{0x} = \mathbf{Y}|_{\hat{x}=0}$, $\mathbf{Z}_{0x} = \mathbf{Z}|_{\hat{x}=0}$, $\mathbf{Y}_{1x} = \mathbf{Y}|_{\hat{x}=1}$ and $\mathbf{Z}_{1x} = \mathbf{Z}|_{\hat{x}=1}$. Manipulation of the cross product gives the desired result:

$$\begin{aligned}\mathbf{Y}\times\mathbf{Z} &= (1-\hat{x})^2(\mathbf{Y}_{0x}\times\mathbf{Z}_{0x}) + \hat{x}^2(\mathbf{Y}_{1x}\times\mathbf{Z}_{1x}) + \hat{x}(1-\hat{x})\left[\mathbf{Y}_{1x}\times\mathbf{Z}_{0x} + \mathbf{Y}_{0x}\times\mathbf{Z}_{1x}\right] \\ &= (1-\hat{x})(\mathbf{Y}_{0x}\times\mathbf{Z}_{0x}) + \hat{x}(\mathbf{Y}_{1x}\times\mathbf{Z}_{1x}) - \hat{x}(1-\hat{x})\left[(\mathbf{Y}_{0x}-\mathbf{Y}_{1x})\times(\mathbf{Z}_{0x}-\mathbf{Z}_{1x})\right]. \qquad (61)\end{aligned}$$

12. APPENDIX B

By (18) and (19) (scaled to an interval of length Δx, with $x/\Delta x$ in the role of $\hat{x}$), along with (21),

$$f_x(x) - Qf_x(x) = \int_0^{\Delta x} G(x,\xi)\, f_x''(\xi)\, d\xi + \frac{x}{\Delta x}\left(1-\frac{x}{\Delta x}\right) f_{2x}\left(\frac{\Delta x}{2}\right). \qquad (62)$$

As the area bounded by the graph of $G(x,\cdot)$ is a triangle of base Δx and (negative) height $x(x/\Delta x - 1)$,

$$\int_0^{\Delta x} G(x,\xi)\, d\xi = \frac{1}{2}x\Delta x\left(\frac{x}{\Delta x}-1\right) = -\frac{1}{2}\Delta x^2\frac{x}{\Delta x}\left(1-\frac{x}{\Delta x}\right). \qquad (63)$$

Combining (62) with (63), we obtain

$$f_x(x) - Qf_x(x) = \int_0^{\Delta x} G(x,\xi)\left[f_x''(\xi) - \frac{2}{\Delta x^2} f_{2x}\left(\frac{\Delta x}{2}\right)\right] d\xi. \qquad (64)$$

We evaluate the bracketed term in (64), differentiating f_x twice, where the appropriate analogue of (16) is

$$f_x(x) = \left(1-\frac{x}{\Delta x}\right) f_{0x}(x) + \frac{x}{\Delta x} f_{1x}(x) - \frac{x}{\Delta x}\left(1-\frac{x}{\Delta x}\right) f_{2x}(x). \qquad (65)$$

This gives

$$\begin{aligned}f_x''(\xi) - \frac{2}{\Delta x^2} f_{2x}\left(\frac{\Delta x}{2}\right) &= -\frac{2}{\Delta x} f_{0x}'(\xi) + \left(1-\frac{\xi}{\Delta x}\right) f_{0x}''(\xi) + \frac{2}{\Delta x^2}\left[f_{2x}(\xi) - f_{2x}\left(\frac{\Delta x}{2}\right)\right] \\ &+ \frac{4}{\Delta x}\left(\frac{\xi}{\Delta x}-\frac{1}{2}\right) f_{2x}'(\xi) - \frac{\xi}{\Delta x}\left(1-\frac{\xi}{\Delta x}\right) f_{2x}''(\xi) + \frac{2}{\Delta x} f_{1x}'(\xi) + \frac{\xi}{\Delta x} f_{1x}''(\xi). \qquad (66)\end{aligned}$$

The expressions in (17a)–(17c) and some rearrangement then yield (22).

13. APPENDIX C

To verify the first relation in (26), define the subelement Q_{xc} of Q, consisting of points $\mathbf{r}(\hat{x},\hat{y},\hat{z})$ for $0 \le \hat{x} \le c$, $0 \le \hat{y} \le 1$, $0 \le \hat{z} \le 1$, and the linear mapping $\mathbf{L}_{xc}(\hat{x},\hat{y},\hat{z}) = (c\hat{x},\hat{y},\hat{z})$. Then $\mathbf{r}\circ\mathbf{L}_{xc}$ maps $\hat{Q}$ to Q_{xc}, $\mathbf{r}\circ\mathbf{L}_{xc}$ is trilinear, and F_{xc} is on the boundary (i.e., is a primary face) of Q_{xc}. Taking $\hat{\mathbf{v}}_{xc}(\hat{x},\hat{y},\hat{z}) = (c\hat{x},0,0)$ on $\hat{Q}$, we apply the Piola transformation (24) to $\mathbf{r}\circ\mathbf{L}_{xc}$ and $\mathbf{r}$ and obtain

$$\begin{aligned}\mathbf{v}_{xc}(\mathbf{r}\circ\mathbf{L}_{xc}(\hat{\mathbf{r}})) &= (J(\mathbf{r}\circ\mathbf{L}_{xc}))(\hat{\mathbf{r}})^{-1}\mathbf{D}(\mathbf{r}\circ\mathbf{L}_{xc})(\hat{\mathbf{r}})\hat{\mathbf{v}}_{xc}(\hat{\mathbf{r}}) = (J(\mathbf{r}\circ\mathbf{L}_{xc}))(\hat{\mathbf{r}})^{-1}\mathbf{D}(\mathbf{r}\circ\mathbf{L}_{xc})(\hat{\mathbf{r}})(c\hat{x},0,0)^T \\ &= [(J(\mathbf{r}))(\mathbf{L}_{xc}(\hat{\mathbf{r}}))c]^{-1}\mathbf{D}\mathbf{r}(\mathbf{L}_{xc}(\hat{\mathbf{r}}))(c^2\hat{x},0,0)^T = (J(r))(L_{xc}(\hat{\mathbf{r}}))^{-1}\mathbf{D}\mathbf{r}(\mathbf{L}_{xc}(\hat{\mathbf{r}}))(c\hat{x},0,0)^T \\ &= (J(r))(L_{xc}(\hat{\mathbf{r}}))^{-1}\mathbf{D}\mathbf{r}(\mathbf{L}_{xc}(\hat{\mathbf{r}}))\hat{\mathbf{v}}(\mathbf{L}_{xc}(\hat{\mathbf{r}})) = \mathbf{v}(\mathbf{r}(\mathbf{L}_{xc}(\hat{\mathbf{r}}))) = \mathbf{v}(\mathbf{r}\circ\mathbf{L}_{xc}(\hat{\mathbf{r}})). \qquad (67)\end{aligned}$$

Thus, the transformed vector-valued functions $\mathbf{v}_{xc}$ and $\mathbf{v}$ take the same values on Q_{xc}, and hence on F_{xc}. Let s denote the variable on F_{xc}, $\hat{\sigma}$ on $\hat{F}_{x1}$, and $\hat{s}$ on $\hat{F}_{xc}$, with $s = \mathbf{r}(\hat{s})$, $\hat{s} = \mathbf{L}_{xc}(\hat{\sigma})$, $s = \mathbf{r}\circ\mathbf{L}_{xc}(\hat{\sigma})$. Now, because

F_{xc} is on the boundary of Q_c, we can use (67), (25), $\hat{\mathbf{v}}_{xc}\cdot\hat{\mathbf{n}}\equiv c$ on $\hat{F}_{x1}$, and the fact that the surface Jacobian of $\mathbf{L}_{xc}$ is 1 on $\hat{F}_{x1}$ to obtain

$$\begin{aligned}\int_{F_{xc}}\mathbf{v}\cdot\mathbf{n}(s)\,z(s)\,ds &= \int_{F_{xc}}\mathbf{v}_{xc}\cdot\mathbf{n}(s)\,z(s)\,ds=\int_{\hat{F}_{x1}}\hat{\mathbf{v}}_{xc}\cdot\hat{\mathbf{n}}(\hat{\sigma})\,z(\mathbf{r}\circ\mathbf{L}_{xc}(\hat{\sigma}))\,d\hat{\sigma}\\ &= \int_{\hat{F}_{x1}}c\,z(\mathbf{r}\circ\mathbf{L}_{xc}(\hat{\sigma}))\,d\hat{\sigma}=\int_{\hat{F}_{xc}}c\,z(\mathbf{r}(\hat{s}))\,d\hat{s},\end{aligned}\tag{68}$$

as desired.

For the second relation in (26), similarly take Q_{yc} to be those $\mathbf{r}(\hat{x},\hat{y},\hat{z})$ for $0\le\hat{x}\le 1$, $0\le\hat{y}\le c$, $0\le\hat{z}\le 1$, $\mathbf{L}_{yc}(\hat{x},\hat{y},\hat{z})=(\hat{x},c\hat{y},\hat{z})$, and $\hat{\mathbf{v}}_{yc}(\hat{x},\hat{y},\hat{z})=(\hat{x},0,0)$ on $\hat{Q}$. Then

$$\begin{aligned}c\mathbf{v}_{yc}(\mathbf{r}\circ\mathbf{L}_{yc}(\hat{\mathbf{r}})) &= (J(\mathbf{r}\circ\mathbf{L}_{yc}))(\hat{\mathbf{r}})^{-1}\,c\mathbf{D}(\mathbf{r}\circ\mathbf{L}_{yc})(\hat{\mathbf{r}})\hat{\mathbf{v}}_{yc}(\hat{\mathbf{r}})=(J(\mathbf{r}\circ\mathbf{L}_{yc}))(\hat{\mathbf{r}})^{-1}\,c\mathbf{D}(\mathbf{r}\circ\mathbf{L}_{yc})(\hat{\mathbf{r}})(\hat{x},0,0)^T\\ &= [(J(\mathbf{r}))(\mathbf{L}_{yc}(\hat{\mathbf{r}}))c]^{-1}\,c\mathbf{D}\mathbf{r}(\mathbf{L}_{yc}(\hat{\mathbf{r}}))(\hat{x},0,0)^T=(J(r))(L_{yc}(\hat{\mathbf{r}}))^{-1}\mathbf{D}\mathbf{r}(\mathbf{L}_{yc}(\hat{\mathbf{r}}))(\hat{x},0,0)^T\\ &= (J(r))(L_{yc}(\hat{\mathbf{r}}))^{-1}\mathbf{D}\mathbf{r}(\mathbf{L}_{yc}(\hat{\mathbf{r}}))\hat{\mathbf{v}}(\mathbf{L}_{yc}(\hat{\mathbf{r}}))=\mathbf{v}(\mathbf{r}(\mathbf{L}_{yc}(\hat{\mathbf{r}})))=\mathbf{v}(\mathbf{r}\circ\mathbf{L}_{yc}(\hat{\mathbf{r}})).\end{aligned}\tag{69}$$

An argument like (68) then yields the second relation in (26).

14. APPENDIX D

We show here that the secondary flux approximation (51), which completes the definition of our velocity shape functions, does not affect the order of accuracy of quadratic flux interpolation. From (17c), (18), and (46), the exact secondary flux to be approximated by $\tilde{f}_{x2}$ is

$$f_{x2}=f_{2x}(1/2)=\int_0^1\int_0^1\mathbf{q}(1/2,\hat{y},\hat{z})\cdot(\mathbf{Y}_{2x}(\hat{z})\times\mathbf{Z}_{2x}(\hat{y}))\,d\hat{y}\,d\hat{z}.\tag{70}$$

As shown in (64), scaled to $\hat{x}$-dimension Δx, the contribution of f_{x2} to the error $(f_x-Qf_x)(x)$ in the quadratic flux interpolation in (22) is

$$Lf_x(x)-Qf_x(x)=\int_0^{\Delta x}G(x,\xi)\left[-\frac{2}{\Delta x^2}f_{x2}\right]d\xi.\tag{71}$$

In (71), integration produces a factor of Δx and $G(x,\xi)=O(\Delta x)$; these factors are canceled by $-2/\Delta x^2$. Thus, to preserve the second-order accuracy of (22), we seek

$$\tilde{f}_{x2}-f_{x2}=O(\Delta x^2).\tag{72}$$

If (72) holds, then the interpolated fluxes Qf_x associated with the velocity approximation $\mathbf{V}_c$ of $\mathbf{q}$ in (46)–(50) will maintain second-order accuracy.

From (51), (52), and (70), we see that

$$\tilde{f}_{x2}-f_{x2} = \int_0^1\int_0^1\left[\frac{1}{8}\sum_{i,j,k=0}^{1}\mathbf{V}_c(i\Delta x,j,k)-\mathbf{q}\left(\frac{\Delta x}{2},\hat{y},\hat{z}\right)\right]\cdot(\mathbf{Y}_{2x}\times\mathbf{Z}_{2x})\,d\hat{y}\,d\hat{z}.\tag{73}$$

Assuming a smooth refinement as in the discussion following (23), $\mathbf{Y}_{2x}$ and $\mathbf{Z}_{2x}$ are $O(\Delta x)$, hence $\mathbf{Y}_{2x}\times\mathbf{Z}_{2x}=O(\Delta x^2)$. The sum in (73) involves discretization in all three directions, so that we must consider refinement in $\hat{y}$ and $\hat{z}$ as well as $\hat{x}$. We seek the error on the $\hat{x}$-face, which is refined in reference space into $1/\Delta y\Delta z$ subfaces of $\hat{y}$-dimension Δy and $\hat{z}$-dimension Δz. By keeping the same relationship between reference and

coarse-cell coordinates, independent of refinement, we keep the same **X**, **Y**, and **Z** vectors and the same Jacobian J (otherwise, we would have to rescale). Thus, on one such subface, we seek

$$\begin{aligned}\tilde{f}_{x2r} - f_{x2r} &= \int_0^{\Delta z}\int_0^{\Delta y}\left[\frac{1}{8}\sum_{i,j,k=0}^{1}\mathbf{V}_c(i\Delta x, j\Delta y, k\Delta z) - \mathbf{q}\left(\frac{\Delta x}{2},\hat{y},\hat{z}\right)\right]\cdot(\mathbf{Y}_{2x}\times\mathbf{Z}_{2x})\,d\hat{y}\,d\hat{z}\\ &= O(\Delta x^2\Delta y\Delta z),\end{aligned} \tag{74}$$

so that the sum of the errors on the subfaces will remain $O(\Delta x^2)$. The estimate that we prove below is

$$\tilde{f}_{x2r} - f_{x2r} = O((\Delta x^2+\Delta y^2+\Delta z^2)\Delta x^2\Delta y\Delta z), \tag{75}$$

which is a much stronger result, showing that the error of the secondary flux approximation is negligible compared to that of quadratic flux interpolation.

Split (74) into two terms T_1 and T_2, replacing $\mathbf{V}_c$ with $\mathbf{q}$ in T_1. Apply the midpoint integration rule in $\hat{y}$ and $\hat{z}$ in T_1 to obtain

$$\begin{aligned}T_1 &= \int_0^{\Delta z}\int_0^{\Delta y}\left[\frac{1}{8}\sum_{i,j,k=0}^{1}\mathbf{q}(i\Delta x, j\Delta y, k\Delta z) - \mathbf{q}\left(\frac{\Delta x}{2},\hat{y},\hat{z}\right)\right](\mathbf{Y}_{2x}\times\mathbf{Z}_{2x})\,d\hat{y}\,d\hat{z}\\ &= \left[\frac{1}{8}\sum_{i,j,k=0}^{1}\mathbf{q}(i\Delta x, j\Delta y, k\Delta z) - \mathbf{q}\left(\frac{\Delta x}{2},\frac{\Delta y}{2},\frac{\Delta z}{2}\right)\right]\cdot\left(\mathbf{Y}_{2x}\left(\frac{1}{2}\right)\times\mathbf{Z}_{2x}\left(\frac{1}{2}\right)\right)\Delta y\Delta z\\ &\quad + O((\Delta y^2+\Delta z^2)\Delta x^2\Delta y\Delta z) \;=\; O((\Delta x^2+\Delta y^2+\Delta z^2)\Delta x^2\Delta y\Delta z),\end{aligned} \tag{76}$$

where the last equality estimates the difference between the sum and the midpoint value of **q**.

For the remaining term of (74), we have

$$\begin{aligned}T_2 &= \int_0^{\Delta z}\int_0^{\Delta y}\left[\frac{1}{8}\sum_{i,j,k=0}^{1}(\mathbf{V}_c - \mathbf{q})(i\Delta x, j\Delta y, k\Delta z)\right]\cdot(\mathbf{Y}_{2x}\times\mathbf{Z}_{2x})\,d\hat{y}\,d\hat{z}\\ &= (E_{0x}+E_{1x}+E_{0y}+E_{1y}+E_{0z}+E_{1z})/2,\end{aligned} \tag{77}$$

where the E terms are associated with the cell faces; for example,

$$E_{0x} = \int_0^{\Delta z}\int_0^{\Delta y}\left[\frac{1}{4}\sum_{j,k=0}^{1}(\mathbf{V}_{\mathbf{X}} - \mathbf{q}_{\mathbf{X}})(0, j\Delta y, k\Delta z)\right]\cdot(\mathbf{Y}_{2x}\times\mathbf{Z}_{2x})\,d\hat{y}\,d\hat{z}. \tag{78}$$

In (78), $\mathbf{q}_{\mathbf{X}}$ and $\mathbf{V}_{\mathbf{X}}$ are multiples of **X**, as in (32) and (50). By construction, with property (UE2) and (46),

$$\mathbf{V}_{\mathbf{X}} = \frac{\mathbf{X}}{J}\beta_{x0}f_{x0} = \frac{\mathbf{X}}{J}\frac{|\mathbf{Y}\times\mathbf{Z}|}{A_x(0)}f_{x0}$$

is defined such that the normal component

$$\mathbf{V}_{\mathbf{X}}\cdot\mathbf{n}_{\hat{x}} = \frac{1}{J}\frac{\mathbf{X}\cdot(\mathbf{Y}\times\mathbf{Z})}{|\mathbf{Y}\times\mathbf{Z}|}\frac{|\mathbf{Y}\times\mathbf{Z}|}{A_x(0)}f_{x0} = \frac{f_{x0}}{A_x(0)} \tag{79}$$

is constant on the face. By (79), $\mathbf{V}_{\mathbf{X}}$ satisfies

$$\frac{1}{4}\sum_{j,k=0}^{1}(\mathbf{V}_{\mathbf{X}}\cdot\mathbf{n}_{\hat{x}})(0, j\Delta y, k\Delta z) = \frac{f_{x0}}{A_x(0)}. \tag{80}$$

Now by (14) and the midpoint integration rule,

$$\begin{aligned}
f_{x0} &= \int_0^{\Delta z}\int_0^{\Delta y} \mathbf{q}_{\mathbf{X}}\cdot(\mathbf{Y}\times\mathbf{Z})\,d\hat{y}\,d\hat{z} \;=\; (\mathbf{q}_{\mathbf{X}}\cdot(\mathbf{Y}\times\mathbf{Z}))(0,\Delta y/2,\Delta z/2)\Delta y\Delta z + O(\Delta y\Delta z(\Delta y^2+\Delta z^2)),\\
A_x(0) &= \int_0^{\Delta z}\int_0^{\Delta y} |\mathbf{Y}\times\mathbf{Z}|\,d\hat{y}\,d\hat{z} \;=\; |\mathbf{Y}\times\mathbf{Z}|(0,\Delta y/2,\Delta z/2)\Delta y\Delta z + O(\Delta y\Delta z(\Delta y^2+\Delta z^2)),\\
\frac{f_{x0}}{A_x(0)} &= \frac{(\mathbf{q}_{\mathbf{X}}\cdot(\mathbf{Y}\times\mathbf{Z}))(0,\Delta y/2,\Delta z/2)}{|\mathbf{Y}\times\mathbf{Z}|(0,\Delta y/2,\Delta z/2)} + O(\Delta y^2+\Delta z^2) \;=\; (\mathbf{q}_{\mathbf{X}}\cdot\mathbf{n}_{\hat{x}})(0,\Delta y/2,\Delta z/2) + O(\Delta y^2+\Delta z^2)\\
&= \frac{1}{4}\sum_{j,k=0}^{1}(\mathbf{q}_{\mathbf{X}}\cdot\mathbf{n}_{\hat{x}})(0,j\Delta y,k\Delta z) + O(\Delta y^2+\Delta z^2). \qquad (81)
\end{aligned}$$

By (80) and (81),

$$\frac{1}{4}\sum_{j,k=0}^{1}((\mathbf{V}_{\mathbf{X}}-\mathbf{q}_{\mathbf{X}})\cdot\mathbf{n}_{\hat{x}})(0,j\Delta y,k\Delta z) = O(\Delta y^2+\Delta z^2). \qquad (82)$$

Now

$$\int_0^{\Delta z}\int_0^{\Delta y}(\mathbf{V}_{\mathbf{X}}-\mathbf{q}_{\mathbf{X}})\cdot\mathbf{n}_{\hat{x}}\,|\mathbf{Y}\times\mathbf{Z}|(0,\hat{y},\hat{z})\,d\hat{y}\,d\hat{z} = f_{x0}-f_{x0}=0,$$

hence for some $(\hat{y}_0,\hat{z}_0)$ we have

$$0=((\mathbf{V}_{\mathbf{X}}-\mathbf{q}_{\mathbf{X}})\cdot\mathbf{n}_{\hat{x}})(\hat{y}_0,\hat{z}_0) = (|\mathbf{V}_{\mathbf{X}}-\mathbf{q}_{\mathbf{X}}|\frac{\mathbf{X}}{|\mathbf{X}|}\cdot\mathbf{n}_{\hat{x}})(\hat{y}_0,\hat{z}_0),$$

whence $(\mathbf{V}_{\mathbf{X}}-\mathbf{q}_{\mathbf{X}})(\hat{y}_0,\hat{z}_0)=0$, which implies that

$$|\mathbf{V}_{\mathbf{X}}-\mathbf{q}_{\mathbf{X}}| = O(\Delta y+\Delta z). \qquad (83)$$

Because $\mathbf{n}_{\hat{x}}(0,j\Delta y,k\Delta z)=\mathbf{n}_{\hat{x}}(0,\Delta y/2,\Delta z/2)+O(\Delta y+\Delta z)$, (82) and (83) give

$$\begin{aligned}
&\frac{1}{4}\sum_{j,k=0}^{1}(\mathbf{V}_{\mathbf{X}}-\mathbf{q}_{\mathbf{X}})(0,j\Delta y,k\Delta z)\cdot\mathbf{n}_{\hat{x}}(0,\Delta y/2,\Delta z/2)\\
&\qquad = O(\Delta y^2+\Delta z^2)+O(\Delta y+\Delta z)O(\Delta y+\Delta z) \;=\; O(\Delta y^2+\Delta z^2),
\end{aligned}$$

from which we immediately obtain

$$\frac{1}{4}\sum_{j,k=0}^{1}|\mathbf{V}_{\mathbf{X}}-\mathbf{q}_{\mathbf{X}}|(0,j\Delta y,k\Delta z) = O(\Delta y^2+\Delta z^2). \qquad (84)$$

Then (78) and (84) yield

$$E_{0x} = O((\Delta y^2+\Delta z^2)\Delta x^2\Delta y\Delta z),$$

and a similar argument for the other five terms in (77) leads to

$$T_2 = O((\Delta x^2+\Delta y^2+\Delta z^2)\Delta x^2\Delta y\Delta z). \qquad (85)$$

Finally, from (76) and (85), we obtain (75), whence

$$\tilde{f}_{x2}-f_{x2} = O((\Delta x^2+\Delta y^2+\Delta z^2)\Delta x^2), \qquad (86)$$

as desired. This is, in fact, a significantly stronger result than (72), showing that the error in the secondary flux approximation is negligible.

If the refinement is not smooth ("random" refinement), then we find that

$$\tilde{f}_{x2} - f_{x2} = O(\Delta x + \Delta y + \Delta z), \tag{87}$$

so that the first-order error in the discussion after (23) is preserved. To see this, trace through the argument above and observe what is lost. The factor Δx^2 is lost throughout because $\mathbf{Y}_{2x} \times \mathbf{Z}_{2x} = O(1)$ instead of $O(\Delta x^2)$. One order is lost in every estimate involving the midpoint rule, because $\mathbf{Y} \times \mathbf{Z}$ or $\mathbf{n}_{\hat{x}}$ can have derivatives of $O(\Delta y^{-1} + \Delta z^{-1})$. One order is lost in (84), because (83) still holds, but $\mathbf{n}_{\hat{x}}$ may vary by $O(1)$.

References

1. Cai, Z., J. E. Jones, S. F. McCormick, and T. F. Russell: 1997, 'Control volume mixed finite element methods'. *Computational Geosciences* **1**, 289–315.
2. Durlofsky, L. J.: 1992, 'A triangle based mixed finite element - finite volume technique for modeling two phase flow through porous media'. *J. Comput. Phys.* **105**, 252–266.
3. Durlofsky, L. J.: 1994, 'Accuracy of mixed and control volume finite element approximations to Darcy velocity and related quantities'. *Water Resour. Res.* **30**(4), 965–973.
4. Naff, R. L., T. F. Russell, and J. D. Wilson: 2000, 'Test functions for three-dimensional control-volume mixed finite-element methods on irregular grids'. In: L. R. Bentley et al. (eds.): *Proceedings of the XIII International Conference on Computational Methods in Water Resources, Calgary, Alberta, Canada, 25-29 June, 2000.* A. A. Balkema, pp. 677–684.
5. Garanzha, V. A. and V. N. Konshin: 1999, 'Approximation schemes and discrete well models for the numerical simulation of the 2-D non-Darcy fluid flows in porous media'. Comm. on appl. math., Computer Centre, Russian Academy of Science, Moscow.
6. Hildebrand, F. B.: 1962, *Advanced Calculus for Applications.* Englewood Cliffs: Prentice-Hall.
7. Arbogast, T., M. F. Wheeler, and I. Yotov: 1997, 'Mixed finite elements for elliptic problems with tensor coefficients as cell-centered finite differences'. *SIAM J. Numer. Anal.* **34**, 828–852.
8. Brezzi, F. and M. Fortin: 1991, *Mixed and Hybrid Finite Element Methods.* New York: Springer-Verlag.
9. Thomas, J. M.: 1977, 'Sur l'analyse numérique des méthodes d'éléments finis hybrides et mixtes'. Thèse d'état, Université Pierre et Marie Curie, Paris.
10. Raviart, P. A. and J. M. Thomas: 1977, 'A mixed finite element method for 2nd order elliptic problems'. In: I. Galligani and E. Magenes (eds.): *Mathematical Aspects of Finite Element Methods*, Vol. 606 of *Lecture Notes in Mathematics.* Springer-Verlag, pp. 292–315.
11. Allen, M. B., R. E. Ewing, and P. Lu: 1992, 'Well-conditioned iterative schemes for mixed finite-element models of porous-media flows'. *SIAM J. Sci. Comput.* **13**(3), 794–814.